Properties of a two-orbital model for oxypnictide superconductors: Magnetic order, B_{2g} spin-singlet pairing channel, and its nodal structure

A. Moreo,[1,2] M. Daghofer,[1,2] J. A. Riera,[3] and E. Dagotto[1,2]
[1]*Department of Physics and Astronomy, The University of Tennessee, Knoxville, Tennessee 37996, USA*
[2]*Materials Science and Technology Division, Oak Ridge National Laboratory, Oak Ridge, Tennessee 32831, USA*
[3]*Instituto de Física Rosario, Consejo Nacional de Investigaciones Científicas y Técnicas, Universidad Nacional de Rosario, 2000-Rosario, Argentina*

(Received 21 January 2009; revised manuscript received 19 February 2009; published 2 April 2009)

A recently proposed two-orbital model for the Fe-based superconductors is studied using the Lanczos method on small clusters as well as pairing mean-field approximations. Our main goals are (i) to provide a comprehensive analysis of this model using numerical techniques with focus on the magnetic state at half-filling and the quantum numbers of the state with two more electrons than half-filling and (ii) to investigate the nodal structure of the mean-field superconducting state and compare the results with angle-resolved photoemission data. In particular, we provide evidence that the dominant magnetic state at half-filling contains spin "stripes," as observed experimentally using neutron scattering techniques. Competing spin states are also investigated. The symmetry properties of the state with two more electrons added to half-filling are also studied: depending on parameters, either a spin-singlet or spin triplet state is obtained. Since experiments suggest spin-singlet pairs, our focus is on this state. Under rotations, the spin-singlet state transforms as the B_{2g} representation of the D_{4h} group. We also show that the $s\pm$ pairing operator transforms according to the A_{1g} representation of D_{4h} and becomes dominant only in an unphysical regime of the model where the undoped state is an insulator. We obtain qualitatively very similar results both with hopping amplitudes derived from a Slater-Koster approximation and with hoppings selected to fit band-structure calculations, the main difference between the two being the size of the Fermi surface pockets. For robust values of the effective electronic attraction producing the Cooper pairs, assumption compatible with recent angle-resolved photoemission spectroscopy (ARPES) results that suggest a small Cooper-pair size, the nodes of the two-orbital model are found to be located only at the electron pockets. Note that recent ARPES efforts have searched for nodes at the hole pockets or only in a few directions at the electron pockets. Thus, our results for the nodal distribution will help us to guide future ARPES experiments in their search for the existence of nodes in the Fe-based superconductors. More in general, the investigations reported here aim to establish several of the properties of the two-orbital model. Only a detailed comparison with experiments will clarify whether this simple model is or not a good approximation to describe the Fe pnictides.

DOI: 10.1103/PhysRevB.79.134502 PACS number(s): 74.20.Mn, 71.27.+a, 71.10.Fd

I. INTRODUCTION

A. Current status of experimental and theoretical investigations

The discovery of a new family of superconducting materials with Fe-As layers in their structure[1–8] has triggered a large effort in the condensed matter community. $LaO_{1-x}F_xFeAs$ is a much studied example of this family of compounds. The ~55 K record critical temperature[7] in $SmO_{1-x}F_xFeAs$ is second only to those observed in the Cu-oxide family of high temperature superconductors. In addition, there are several aspects of the physics of the Fe-based superconductors that suggest the possibility of an exotic pairing mechanism at work:

(1) Evidence is accumulating that phonons may not be sufficient to understand the superconductivity of these compounds.[9–11] Moreover, the importance of correlations between the electrons has been remarked in several investigations.[12–22] In fact, it has been claimed that these oxypnictide superconductors may bridge the gap between MgB_2 and the Cu-oxide superconductors.[23,24] In addition, a pseudogap was detected, similarly as in the cuprates.[25–28] Coexistence or proximity of magnetism and superconductivity has also been reported.[29–32] Although the parent undoped compound is not a Mott insulator, these results suggest that the influence of electron-electron repulsions cannot be neglected. Perhaps the *intermediate* range of U/t, where U is the typical Hubbard repulsion scale and t is the typical hopping amplitude in a tight-binding description, is the most representative of the Fe-based superconductors. U cannot be too large, otherwise the system would develop a gap and the undoped compound would be insulating, contrary to the experimentally observed properties of the undoped limit that suggest bad metallic behavior. But poor-metal characteristics imply that U cannot be too small either, otherwise the undoped system would be a good metal. In addition, the mere presence of a spin-density-wave magnetic state shows that correlations must be important.

(2) Several experimental investigations suggest the presence of nodes in the superconducting gap.[33–43] This is reminiscent of the nodes that appear in the d-wave superconducting state of the high-T_c cuprates. However, other investigations indicate nodeless superconductivity.[44–50] As a consequence, this issue is still controversial.

(3) The undoped parent compound has long-range spin order in the ground state.[51] This magnetic state corresponds

to spin "stripes" having the Fe spins along one of the Fe-Fe crystal axes pointing all in the same direction and being antiferromagnetically coupled in the perpendicular direction. According to neutron scattering experiments, in LaOFeAs the transition to this magnetic state occurs at 134 K and the magnetic moment is $0.36\mu_B$, which is smaller than anticipated.[52] For NdOFeAs,[53] the critical temperature is 141 K and the magnetic moment is even smaller, $0.25\mu_B$. However, recently by means of resistivity, specific heat, and magnetic susceptibility measurements, the antiferromagnetic critical temperature of $SrFe_2As_2$ was reported to be as high as 205 K, with a more robust Fe magnetic moment of value of $1.7\mu_B$.[54] Also, $CaFe_2As_2$ was investigated using neutron diffraction, and a critical temperature of 173 K with a moment of $0.8\mu_B$ was reported.[55] Thus, although originally it was believed that the undoped material had a very weak magnetic state, the most recent results suggest that the spin-striped order may be more robust.

On the theory front, several band-structure calculations have shown that the Fermi surface (FS) of these and related compounds is made out of two small hole pockets centered at the Γ point and small electron pockets at the X and Y points, in the notation corresponding to a square lattice of Fe atoms.[56–60] These calculations have also shown that the $3d$ levels of Fe play the dominant role in establishing the properties of these materials near the Fermi level. To address theoretically the physics of these compounds, particularly the superconducting state, model Hamiltonians are needed and several proposals for the dominant pairing tendencies have been made.[61–72] In particular, a two-orbital model based on the d_{xz} and d_{yz} orbitals was recently presented.[73] Several other investigations have addressed this model for the Fe-based superconductors, using a variety of approximations.[74–85] Classifications of the possible superconducting order parameters for the two-orbital model have been made.[86–89]

As already mentioned, a variety of experimental results suggests that the Cooper pairs are spin singlets.[38,40,90] Thus, it is important to find the range of parameters leading to spin singlets in model Hamiltonians since several calculations produce either singlet or triplet superconductivity depending on the couplings and bandwidths used. For this experimentally based reason, our focus here will be mainly on singlet superconductivity.

B. Why the two-orbital model?

In this paper, a detailed study of the two-orbital model for the oxypnictide superconductors is carried out using Lanczos and pairing mean-field (MF) techniques. This effort provides a comprehensive view of the model, considerably expanding our recent research on the subject[76] by varying the several couplings of the model and studying the main tendencies. When two electrons are added to the half-filled ground state, a spin-singlet state that transforms in a nontrivial manner under rotations is shown to dominate in the regime of couplings that is argued to be the most relevant to describe the superconductors. In addition, the nodal structure of the Fe-based superconducting state obtained using these spin-singlet pairs is here studied for this model using the pairing mean-field approximation. Our results are compared with recent angle-resolved photoemission spectroscopy (ARPES) experiments, and suggestions to further refine the search for nodes in those experiments are discussed.

Currently there is no consensus on what is the minimal model capable of capturing the essential physics of the oxypnictides. Band structure calculations in the local-density approximation (LDA) indicate that the bands that form the observed electron and hole pockets are strongly hybridized but they have mostly Fe $3d$ character.[62,91] Several authors argue that the hybridization of the Fe $3d$ is so strong that all five d orbitals have to be considered to construct a minimal model. For instance, a five-orbital model has been proposed.[61] The tight-binding term respects the FeAs lattice symmetries and the hopping parameters have been obtained from fittings against the LDA calculations. The parameters used reproduce the FS for the electron doped system (i.e., electronic density $n=6.1$) but an extra hole pocket around M [in the notation of the extended Brillouin zone (BZ)] appears for the undoped case and upon hole doping. For this reason, the model may not be suitable to study the magnetic properties of the undoped system. In addition, the number of degrees of freedom in five-orbital models makes its study very difficult using numerical techniques. However, LDA calculations have shown that, although heavily hybridized, the main characters of the bands that determine the FS are d_{xz} and d_{yz}, with a small contribution of d_{xy} at the most elongated portions of the electron pockets.[60,91] This fact has been the main justification for the proposal of two-[73,76] and three-orbital[67] models. The two-orbital model can have its hopping parameters fitted such that the shape of the FS, both in the undoped and electron and hole doped cases, is well reproduced in the reduced or folded BZ. However, it has been argued by some authors[67] that the two hole pockets around Γ have to arise from the d_{xz} and d_{yz} orbitals that are degenerate with each other at Γ, as obtained in LDA. In the two-orbital model, one of the hole pockets forms around M in the extended BZ which gets mapped onto Γ upon folding. The d_{xz} and d_{yz} orbitals that form the M-point pocket are degenerate at M and, upon the folding, give rise to higher energy bands at the Γ point. For this reason one of the hole pockets in the two-orbital model may not have the correct linear combination of orbitals, potentially leading to incorrect conclusions. In addition, it is also argued that the contribution of the d_{xy} orbital to the electron pockets may play an important role that should not be ignored which motivated the proposal of the three-orbital model.[67] However, the three-orbital model cannot eliminate a spurious hole pocket around M. Thus, a fourth-orbital needs to be added to accomplish this task and, again, the number of degrees of freedom makes this model too complex to be studied numerically.

Then, the justifications for continuing studying a minimal model with just *two* orbitals, as carried out in the present paper, are the following: (i) The correct shape of the FS is reproduced in the *reduced* Brillouin zone, both in the doped and undoped cases. (ii) The main characters of all the bands that determine the FS are d_{xz} and d_{yz}, except for a small portion of the electron pockets that has d_{xy} character. Then, it is worthwhile to understand the role, if any, that this orbital plays in the magnetic and superconducting states. (iii) The two-orbital model is the only one that can be studied exactly with numerical techniques using the minimal size cluster needed for a spin-striped state.[76] Thus, we believe that it is very important to establish which properties of the oxypnictides are properly captured by this model and which one is not. The role that the correct shape of the FS plays can be investigated as well and also the pairing symmetry and nodal structure involving only the d_{xz} and d_{yz} orbitals. It is interesting to note that although two superconducting gaps may appear in a two-orbital model,[92] symmetry forces the magnitude of the gaps to be the same in this case.[89]

C. Organization

The organization of the paper is as follows. In Secs. II and III, the two-orbital model is derived. The emphasis is on the Slater-Koster (SK) procedure to evaluate the hopping amplitudes, but the model derived by this method is more general: it coincides with the two-orbital Hamiltonian proposed earlier,[73] and the values of the hoppings can be obtained also by fitting band-structure calculations.[73] Both sets of hopping parameters will be used in Secs. II–V. The qualitative aspects of the magnetic and pairing states are shown to be the same for both sets of hopping amplitudes. In Sec. IV, results for the ground states of the undoped model (half-filled) and the case of two more electrons than half-filling will be discussed using the Lanczos technique. The emphasis is on the dominant magnetic states and on the pairing tendencies, which are either in the spin-singlet or triplet channels depending on couplings. Moreover, the spin-singlet case is shown to correspond to the B_{2g} representation of the D_{4h} lattice symmetry group of the model. Section V contains a pairing mean-field analysis of the nodal structure of the model. The two-orbital nature of the problem causes the number and location of the nodes to be a more complex topic than for just one orbital. A qualitative comparison with experiments is included here. Section VI contains our main conclusions. The possible sources of the B_{2g} pairing and the $s\pm$ pairing operator are discussed in Appendixes A and B.

II. MODEL DISCUSSION AND DERIVATION OF HOPPING AMPLITUDES

To study numerically the properties of $LaO_{1-x}F_xFeAs$ and related compounds, it is necessary to construct a simple model, one that contains a minimum amount of degrees of freedom but still preserves the main physics of the problem. Since all the materials in the family have in common the Fe-X planes (X=As,P,…), as a first approximation we will just focus on those planes, similarly as it occurs in theoretical studies of the Cu-O planes in the cuprate superconductors. In addition, band-structure calculations[56–60] have shown the relevance of the Fe 3d levels and that mainly two bands determine the Fermi surface (see Sec. I). Based on these considerations, here we will include only the d_{xz} and d_{yz} Fe orbitals in our discussion. To estimate the hopping amplitudes for the tunneling from one Fe to another and, thus, define a tight-binding model, we will calculate their hybridization with the three p orbitals of As following the Slater-Koster formalism.[93] From the Fe-As hopping integrals, we will calculate the effective Fe-Fe tight-binding hopping parameters following a standard perturbative approach. Thus, the hopping parameters in this model will be functions of the overlap integrals between the orbitals and the distance between the atoms. While this procedure is not as accurate as band-structure calculations, it provides a simple to understand approach that has *ab initio* characteristics, which can be easily reproduced since the calculations are analytical, and they also illustrate how the geometry of the problem affects the hoppings.

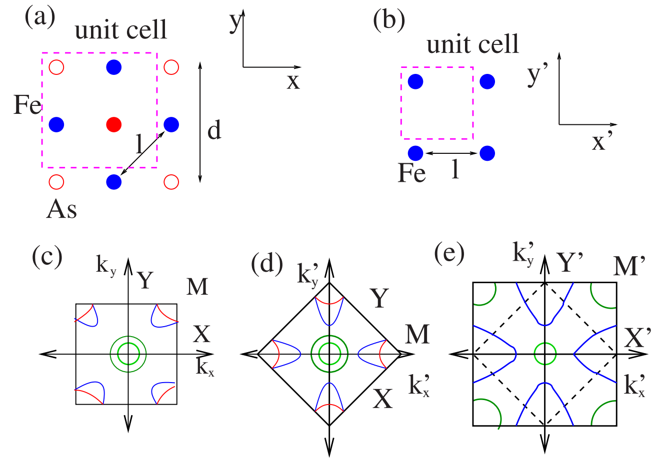

FIG. 1. (Color online) (a) Schematic representation of the Fe-As plane. Blue circles are the Fe atoms. The red filled circle is an As atom at a distance c below the plane, while the red open circles are As atoms at a distance c above the plane. (b) Unit cell for the effective Fe-only square lattice. The Fe-Fe lattice has been rotated by 45°. (c) Schematic first Brillouin Zone (FBZ) for the Fe-As plane. The point X is at $(2\pi/d,0)$, with $d=\sqrt{2}l$. (d) FBZ for the Fe-As lattice after a 45° rotation. (e) FBZ for the rotated Fe-Fe shown in (b). $X'=(2\pi/l,0)$ and it is equivalent to the M point for the Fe-As plane in (c). The electron and hole Fermi surfaces obtained by band-structure calculations are schematically indicated. Panels (c)–(e) will be useful for the discussion related to the nodal structure of the superconducting state in Sec. V.

However, before proceeding, we remark that another avenue to obtain the hopping amplitudes is via fittings of the band-structure calculations.[73] In our description of results below, data for both the SK hoppings and those that fit band structures will be presented. An important result is that both sets of hoppings lead to similar qualitative results, both in the undoped case, regarding the magnetic state, as for two electrons added, regarding the pairing tendencies.

The unit cell in the FeAs planes contains two Fe atoms since the As atoms are above and below the plane defined by the Fe atoms in alternating plaquettes [Fig. 1(a)]. However, after the calculation previously described only the Fe atoms will be considered in a simple two-orbital Hamiltonian. Since these Fe atoms form a planar square lattice, it is natural to orient the lattice as in Fig. 1(b).

To guide the discussion, consider a cluster with four Fe and five As atoms [Fig. 2(a)]. The coordinates of the atoms are needed to calculate hopping amplitudes, and they are

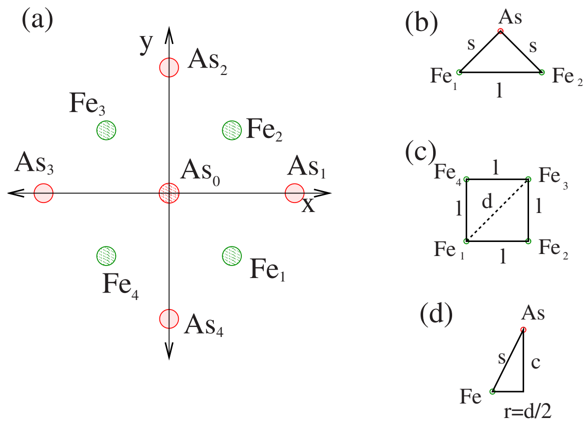

FIG. 2. (Color online) (a) The Fe-As cluster used in our calculations of the hoppings. Green circles are the Fe atoms. The red circle at the center is an As atom at a distance c below the plane, while the shaded red circles are the As atoms that are a distance c above the plane. (b) Distances s and l for NN Fe-Fe atoms. (c) The distance d along the diagonal of the Fe-Fe plaquettes. (d) The distance c for As atoms.

provided in Table I, where k, l, and c are obtained from the materials structure. The nearest-neighbor (NN) Fe-Fe distance is $l=2.854$ Å,[57] thus $k=l/2=1.427$ Å. The distance between Fe and As is $s=2.327$ Å (Ref. 57) [see Fig. 2(b)]. The next-nearest-neighbor (NNN) Fe-Fe distance along the square diagonal is $d=\sqrt{2}l=4.037$ Å [see Fig. 2(c)] and $r=d/2=2.018$ Å. According to Fig. 2(d), $c=\sqrt{s^2-r^2}=\sqrt{s^2-l^2/2}=1.158$ Å. The director cosines l, m, and n for each of the Fe atoms,[93] with respect to the As located at $(0,0,-c)$, are given in Table II.

A. Overlap integrals between the Fe d_{xz} and d_{yz} orbitals and the As p_x and p_y orbitals

According to the SK analysis, for the orbitals considered here we obtain the following results for the center integrals,

$$E_{x,yz}=\sqrt{3}lmn(pd\sigma)-2lmn(pd\pi), \tag{1}$$

$$E_{y,xz}=\sqrt{3}lmn(pd\sigma)-2lmn(pd\pi), \tag{2}$$

$$E_{x,xz}=\sqrt{3}l^2n(pd\sigma)+n(1-2l^2)(pd\pi), \tag{3}$$

TABLE I. Coordinates of the atoms in Fig. 2(a).

Ion	x	y	z
As_0	0	0	$-c$
Fe_1	k	$-k$	0
Fe_2	k	k	0
Fe_3	$-k$	k	0
Fe_4	$-k$	$-k$	0
As_1	1	0	c
As_2	0	1	c
As_3	$-l$	0	c
As_4	0	$-l$	c

TABLE II. Director cosines of the Fe atoms with respect to As_0 in Fig. 2(a).

Ion	l	m	n
Fe_1	k/s	$-k/s$	c/s
Fe_2	k/s	k/s	c/s
Fe_3	$-k/s$	k/s	c/s
Fe_4	$-k/s$	$-k/s$	c/s

$$E_{y,yz}=\sqrt{3}m^2n(pd\sigma)+n(1-2m^2)(pd\pi). \tag{4}$$

The corresponding hopping amplitudes are

$$|t_{x,yz}|=|t_{y,xz}|=a=\sqrt{3}\frac{k^2c}{s^3}(pd\sigma)-2\frac{k^2c}{s^3}(pd\pi), \tag{5}$$

$$|t_{x,xz}|=|t_{y,yz}|=b=\sqrt{3}\frac{k^2c}{s^3}(pd\sigma)+\frac{c}{s}\left(1-2\frac{k^2}{s^2}\right)(pd\pi). \tag{6}$$

The signs and values of these hoppings for the cluster that we are considering are in Fig. 3. The values of l, m, and n shown in Table I are for As_0, while some signs will be different for As_1, As_2, As_3, and As_4.

Using the values of k, s, and c given above, we obtain

$$a=0.324(pd\sigma)-0.374(pd\pi), \tag{7}$$

$$b=0.324(pd\sigma)+0.123(pd\pi). \tag{8}$$

Now let us compute the hopping amplitudes for a square lattice made up only of Fe atoms. For the NN effective Fe-Fe hopping t_{NN} we will consider the pair of atoms Fe_1 and Fe_2. For the hopping between the d_{xz} orbitals, there are two possible paths using the As p_y as a bridge. Their contribution is given by (1) $d_{xz}Fe_1$-p_yAs_0-$d_{xz}Fe_2$ and (2) $d_{xz}Fe_1$-p_yAs_1-$d_{xz}Fe_2$. From Fig. 3(a), we observe that these paths contribute with $-a^2$ each. Regarding the use of the p_x of As as a bridge, in this case there are also two paths: (3) $d_{xz}Fe_1$-p_xAs_0-$d_{xz}Fe_2$ and (4) $d_{xz}Fe_1$-p_xAs_1-$d_{xz}Fe_2$. From Fig. 3(b), these paths contribute with b^2 each. Reasoning in an analogous manner, four similar paths are found for the NN

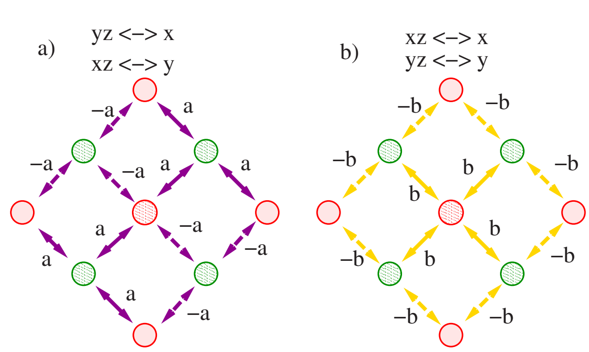

FIG. 3. (Color online) (a) Hoppings between $d_{yz}(d_{xz})$ orbitals in Fe and $p_x(p_y)$ orbitals in As for the cluster considered in Fig. 2(a). (b) Hoppings between $d_{yz}(d_{xz})$ orbitals in Fe and $p_y(p_x)$ orbitals in As for the cluster considered in Fig. 2(a). Continuous (dashed) lines indicate positive (negative) values.

hopping between orbitals d_{yz}: (1) $d_{yz}Fe_1$-p_xAs_0-$d_{yz}Fe_2$ and (2) $d_{yz}Fe_1$-p_xAs_1-$d_{yz}Fe_2$, which from Fig. 3(a) they give a contribution $-a^2$ each, and (3) $d_{yz}Fe_1$-p_yAs_0-$d_{yz}Fe_2$ and (4) $d_{yz}Fe_1$-p_yAs_1-$d_{yz}Fe_2$, which from Fig. 3(b) they give a contribution b^2 each. Combining all these results, and to second order in perturbation theory,[94] the Fe-Fe nearest-neighbor hopping amplitude is given by

$$t^{xz}_{\mathrm{NN}} = t^{yz}_{\mathrm{NN}} = (-2a^2 + 2b^2)/\Delta = 2(b^2 - a^2)/\Delta, \tag{9}$$

where Δ is the difference between the on-site energies of the d and p orbitals. Notice that by mere geometrical reasons, it is not possible to have a nearest-neighbor hopping from d_{yz} to d_{xz}.

For the hopping t_d along the Fe lattice plaquette diagonal, namely, the NNN Fe-Fe hopping, let us consider the hopping from Fe_1 to Fe_3 and from Fe_2 to Fe_4. It can be easily shown that $d_{xz}Fe_1$-p_xAs_0-$d_{xz}Fe_3$ contributes by an amount b^2 to t_d^{xz}, while $d_{xz}Fe_1$-p_yAs_0-$d_{xz}Fe_3$ contributes a^2 to t_d^{xz}. The same result is obtained if the hopping from Fe_2 to Fe_4 is considered. Combining these numbers, then we obtain $t_d^{xz}=t_d^{yz}=(a^2+b^2)/\Delta$.

Along the plaquette diagonal we can also obtain interorbital hopping. From Fe_1 to Fe_3 the contribution is $-ab$, while from Fe_2 to Fe_4 it is ab. Thus, the hoppings along the $x+y$ and $x-y$ directions are different by a sign from the interorbital hopping. The fact that the plaquette diagonals are equivalent by symmetry implies that the absolute values of the hoppings must be the same along these diagonals, but the signs can be different as shown here. More explicitly, we obtain $t_{x+y}^{xz-yz}=ab/\Delta$, and $t_{x-y}^{xz-yz}=-ab/\Delta$.

B. Overlap between d_{xz} and d_{yz} with p_z

The consideration of the p_z orbitals adds two center integrals to the present analysis:

$$E_{z,xz} = \sqrt{3}n^2 l(pd\sigma) + l(1-2n^2)(pd\pi), \tag{10}$$

$$E_{z,yz} = \sqrt{3}n^2 m(pd\sigma) + m(1-2n^2)(pd\pi), \tag{11}$$

which means that an additional hopping must be considered

$$|t_{z,xz}| = |t_{z,yz}| = g = \sqrt{3}\frac{kc^2}{s^3}(pd\sigma) + \frac{k}{s}\left(1 - 2\frac{c^2}{s^2}\right)(pd\pi). \tag{12}$$

Using the values for k, s, and c calculated before,

$$g = 0.263(pd\sigma) + 0.31(pd\pi). \tag{13}$$

The signs are indicated in Figs. 4(a) and 4(b).

Thus, we obtain an additional contribution to the NN hopping t_{NN} so that $t^{xz}_{\mathrm{NN}}=2g^2/\Delta'(-2g^2/\Delta')$ along the y (x) axis. Reciprocally, $t^{yz}_{\mathrm{NN}}=2g^2/\Delta'(-2g^2/\Delta')$ along the x (y) axis. Along the diagonal, $t_d=-g^2/\Delta'$ for both orbitals is obtained. Note also that p_z generates an interorbital diagonal hopping given by $-g^2/\Delta'$ (g^2/Δ') along the $x+y$ $(x-y)$ directions. Δ' is the difference between the on-site energies of the d and p_z orbitals. From Ref. 59, the gaps are $\Delta=1.25$ eV and $\Delta'=5$ eV, but other values for these gaps are also considered below.

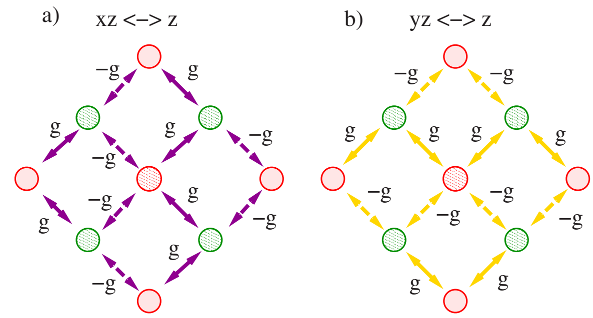

FIG. 4. (Color online) (a) Hoppings between the d_{yz} orbitals in Fe and the p_z orbitals in As for the cluster considered in Fig. 2(a). (b) Hoppings between the d_{xz} orbitals in Fe and the p_z orbitals in As for the cluster considered in Fig. 2(a). Continuous (dashed) lines indicate positive (negative) values.

C. Direct Fe-Fe hopping

Since the distance between Fe atoms is $l=2.854$ Å, comparable to the Fe-As distance, the contributions to the electron hoppings coming from the direct overlap between the d orbitals of the Fe atoms should also be considered. Following SK,[93] $E_{xz,xz}=3l^2n^2(dd\sigma)+(l^2+n^2-4l^2n^2)(dd\pi)+(m^2+l^2n^2)dd\delta$, $E_{yz,yz}=3m^2n^2(dd\sigma)+(m^2+n^2-4m^2n^2)(dd\pi)+(l^2+m^2n^2)dd\delta$, and $E_{xz,yz}=3lmn^2(dd\sigma)+lm(1-4n^2)[(dd\pi)-(dd\delta)]$. Notice that all the Fe atoms have $n=0$ and $l=\pm 1$, $m=0(l=0,m=\pm 1)$ if they are neighbors along the $x(y)$ direction. Thus, the interorbital hopping vanishes, and we obtain $t_{xz,xz}=-dd\pi(t_{yz,yz}=-dd\pi)$ along the direction $x(y)$ and $dd\delta$ along $y(x)$. These same expressions can be used to obtain the diagonal Fe-Fe hopping parameters. We find that $t^d_{\alpha,\alpha}=-(dd\pi'+dd\delta')/2$, where $\alpha=xz$ or yz, while $t^d_{xz,yz}=\pm(dd\pi'-dd\delta')/2$ with the minus (plus) sign for the $\hat{x}+\hat{y}$ $(\hat{x}-\hat{y})$ direction and the prime indicates second-nearest-neighbor overlap integrals.

III. EFFECTIVE TWO-ORBITAL TIGHT-BINDING MODEL

A. Hopping term

Considering the results of Sec. II C, the kinetic-energy term of the effective tight-binding Hamiltonian involving the d_{xz} and d_{yz} orbitals, defined on the square lattice formed only by the Fe atoms, is given by

$$\begin{aligned}
H_{\mathrm{TB}} = &- t_1 \sum_{\mathbf{i},\sigma} (d^\dagger_{\mathbf{i},x,\sigma} d_{\mathbf{i}+\hat{y},x,\sigma} + d^\dagger_{\mathbf{i},y,\sigma} d_{\mathbf{i}+\hat{x},y,\sigma} + \mathrm{H.c.}) \\
&- t_2 \sum_{\mathbf{i},\sigma} (d^\dagger_{\mathbf{i},x,\sigma} d_{\mathbf{i}+\hat{x},x,\sigma} + d^\dagger_{\mathbf{i},y,\sigma} d_{\mathbf{i}+\hat{y},y,\sigma} + \mathrm{H.c.}) \\
&- t_3 \sum_{\mathbf{i},\hat{\mu},\hat{\nu},\sigma} (d^\dagger_{\mathbf{i},x,\sigma} d_{\mathbf{i}+\hat{\mu}+\hat{\nu},x,\sigma} + d^\dagger_{\mathbf{i},y,\sigma} d_{\mathbf{i}+\hat{\mu}+\hat{\nu},y,\sigma} + \mathrm{H.c.}) \\
&+ t_4 \sum_{\mathbf{i},\sigma} (d^\dagger_{\mathbf{i},x,\sigma} d_{\mathbf{i}+\hat{x}+\hat{y},y,\sigma} + d^\dagger_{\mathbf{i},y,\sigma} d_{\mathbf{i}+\hat{x}+\hat{y},x,\sigma} + \mathrm{H.c.}) \\
&- t_4 \sum_{\mathbf{i},\sigma} (d^\dagger_{\mathbf{i},x,\sigma} d_{\mathbf{i}+\hat{x}-\hat{y},y,\sigma} + d^\dagger_{\mathbf{i},y,\sigma} d_{\mathbf{i}+\hat{x}-\hat{y},x,\sigma} + \mathrm{H.c.}) \\
&- \mu \sum_{\mathbf{i}} (n^x_{\mathbf{i}} + n^y_{\mathbf{i}}).
\end{aligned} \tag{14}$$

In this Hamiltonian, the operator $d^{\dagger}_{\mathbf{i},\alpha,\sigma}$ creates an electron with spin z-axis projection σ, orbital α, and on the site $\mathbf{i}$ of a square lattice. The chemical potential is given by μ and $n^{\alpha}_{\mathbf{i}}$ are number operators. The index $\hat{\mu}=\hat{x}$ or $\hat{y}$ is a unit vector linking nearest-neighbor sites. The hoppings, within the SK approach, are given by

$$t_1 = -2[(b^2-a^2)/\Delta + g^2/\Delta'] - dd\delta,$$

$$t_2 = -2[(b^2-a^2)/\Delta - g^2/\Delta'] - dd\pi,$$

$$t_3 = -[(a^2+b^2\Delta - g^2/\Delta')] - (dd\pi' + dd\delta')/2,$$

$$t_4 = -(ab/\Delta - g^2/\Delta') - (dd\pi' - dd\delta')/2. \tag{15}$$

The explicit expressions for these hopping amplitudes in terms of the overlap integrals using the parameters for FeAs can be easily found and they will not be provided here. The two-orbital model proposed by Raghu *et al.*[73] has the same form as the one presented above but the hoppings are obtained by fitting band structures.[60]

It is interesting to note that if only the direct overlap between the d orbitals is considered, i.e., ignoring the indirect hopping through the p As orbitals, the form of Eq. (14) does not change. Thus, the form of H_{TB} arises from the symmetry properties of the d_{xz} and d_{yz} orbitals rather than from the location of the As ions. However, the indirect Fe-Fe hopping through the As atoms plays a key role in providing the relatively large value of the diagonal hopping t_3 vs the NN hoppings which, as discussed below, stabilizes the magnetic stripe order. For example, if we only consider the direct hopping then $t_3/t_2 \approx dd\pi'/2dd\pi$, where $dd\delta' \approx 0$ was assumed.[95] Since $dd\pi' \ll dd\pi$, then $|t_3| \ll |t_2|$. However, if we consider the indirect hopping then $|t_3| \geq |t_2|/2$.

To analyze the influence of the several parameters, let us consider two special cases. Setting $(pd\sigma)=1.0$ eV, $pd\pi=-0.2$ eV, $\Delta=1.0$ eV, and $\Delta'=1$ eV in Eqs. (15)–(18), and neglecting the direct Fe-Fe coupling i.e., using $dd\pi=dd\delta=0$, we obtain $t_1=0.058$ eV, $t_2=0.22$ eV, $t_3=-0.21$ eV, and $t_4=-0.08$ eV. With these values, the band structure, shown in Fig. 5, is qualitatively similar to the band-structure calculations, although the pockets are larger in size. Another example can be obtained by using the calculated values of the energy gaps, which are $\Delta=1.25$ eV and $\Delta'=5$ eV.[59] In Fig. 6, the band structure is shown for $(pd\sigma)=1$ eV, $pd\pi=-0.2$ eV, $\Delta=1.25$ eV, $\Delta'=5$ eV, $dd\pi=0.2$ eV, and $dd\delta=-0.02$ eV, i.e., including the direct Fe-Fe hopping. Now the hole pocket at Γ is larger than in the previous case, but the overall shape remains similar.

Notice that the overlap integrals can also be estimated using tabulated values and the distances between the atoms.[95] The band structure and Fermi surface obtained using these values are shown in Fig. 7.

To complete the analysis, let us discuss now the results obtained using the set of hoppings that fit band-structure calculations.[73] The dispersion and Fermi surface are in Fig. 8. By construction, the agreement with the band-structure Fermi surface is better than in the other cases, the main difference being the size of the pockets. Nevertheless, it appears that in a broad range of hoppings and couplings, the qualitative topology of the Fermi surfaces remains the same, and this is probably the reason why the main magnetic and pairing properties are also similar among the many sets, as shown explicitly below.

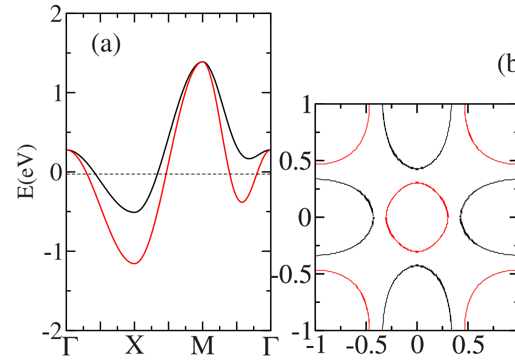

FIG. 5. (Color online) (a) Energy vs momentum for the noninteracting tight-binding Hamiltonian in Eq. (14) using $t_1=0.058$ eV, $t_2=0.22$ eV, $t_3=-0.21$ eV, and $t_4=-0.08$ eV. These hopping amplitudes are obtained from the Slater-Koster formulas using $(pd\sigma)=1$ eV and $(pd\pi)=-0.2$ eV, supplemented by $\Delta=\Delta'=1$ eV for simplicity, and $\mu=-0.03$ eV, which corresponds to half-filled orbitals. Results are plotted along the path $(0,0)-(\pi,0)-(\pi,\pi)-(0,0)$. (b) Fermi surface for the half-filled system.

B. Interactions

In this section, the Coulombic interaction terms are added to the tight-binding Hamiltonian (14) to form the full two-orbital model. These Coulombic terms are[76]

$$H_{\mathrm{int}} = U\sum_{\mathbf{i},\alpha} n_{\mathbf{i},\alpha,\uparrow}n_{\mathbf{i},\alpha,\downarrow} + (U'-J/2)\sum_{\mathbf{i}} n_{\mathbf{i},x}n_{\mathbf{i},y} - 2J\sum_{\mathbf{i}} \mathbf{S}_{\mathbf{i},x}\cdot\mathbf{S}_{\mathbf{i},y} + J\sum_{\mathbf{i}} (d^{\dagger}_{\mathbf{i},x,\uparrow}d^{\dagger}_{\mathbf{i},x,\downarrow}d_{\mathbf{i},y,\downarrow}d_{\mathbf{i},y,\uparrow+\mathrm{H.c.}}), \tag{16}$$

where $\alpha=x,y$ denotes the orbital, $\mathbf{S}_{\mathbf{i},\alpha}$ ($n_{\mathbf{i},\alpha}$) is the spin (electronic density) in orbital α at site $\mathbf{i}$, and we have used the

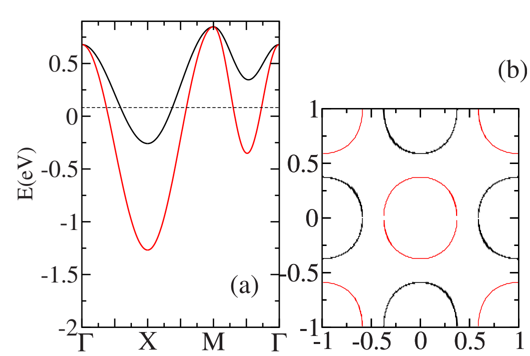

FIG. 6. (Color online) (a) Energy vs momentum for the noninteracting tight-binding Hamiltonian (14) using $t_1=-0.1051$ eV, $t_2=0.1472$ eV, $t_3=-0.1909$ eV, and $t_4=-0.0874$ eV, obtained using the parameters $(pd\sigma)=1$ eV, $(pd\pi)=-0.2$ eV, $dd\pi=0.2$ eV, $dd\delta=-0.02$ eV, $\Delta=1.25$ eV, and $\Delta'=5$ eV. The chemical potential is $\mu=0.081$ eV, which corresponds to half-filled orbitals. Results are plotted along the path $(0,0)-(\pi,0)-(\pi,\pi)-(0,0)$. (b) Fermi surface for the half-filled system.

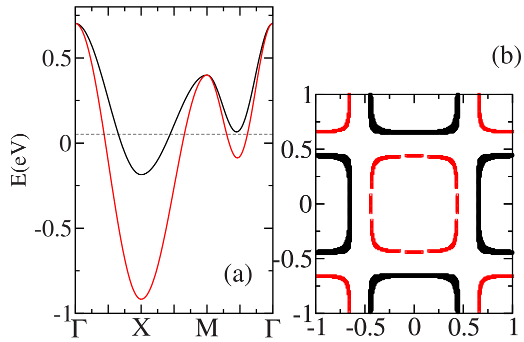

FIG. 7. (Color online) (a) Energy vs momentum for the noninteracting tight-binding Hamiltonian in Eq. (14) using $t_1 = -0.129$ eV, $t_2 = 0.05$ eV, $t_3 = -0.137$ eV, and $t_4 = -0.019$ eV obtained for $(pd\sigma) = -0.41$ eV, $(pd\pi) = 0.19$ eV, $dd\pi = 0.18$ eV, $dd\delta = 0$, $\Delta = 1.25$ eV, and $\Delta' = 5$ eV. The chemical potential is $\mu = 0.053$ eV, which corresponds to half-filled orbitals. Results are plotted along the path $(0,0)-(\pi,0)-(\pi,\pi)-(0,0)$. (b) Fermi surface for the half-filled system.

relation $U' = U - 2J$ from rotational invariance.[96]

C. Pairing

Diagonalizing exactly the full two-orbital Hamiltonian on a $\sqrt{8} \times \sqrt{8}$ cluster with periodic boundary conditions, it was observed in previous investigations that in regions of parameter space the ground state with two extra electrons above half-filling is a spin triplet.[76] In this case, the relevant pairing operator is given by

$$\Delta^{\dagger}(\mathbf{i})_{\sigma} = \sum_{\mu} (d^{\dagger}_{\mathbf{i},x,\sigma} d^{\dagger}_{\mathbf{i}+\mu,y,\sigma} - d^{\dagger}_{\mathbf{i},y,\sigma} d^{\dagger}_{\mathbf{i}+\mu,x,\sigma}), \tag{17}$$

where $\sigma = \uparrow$ or $\downarrow$ denotes the spin projection 1 or -1, respectively, while the 0 projection operator is

$$\Delta^{\dagger}(\mathbf{i})_0 = \sum_{\mu} (d^{\dagger}_{\mathbf{i},x,\uparrow} d^{\dagger}_{\mathbf{i}+\mu,y,\downarrow} + d^{\dagger}_{\mathbf{i},x,\downarrow} d^{\dagger}_{\mathbf{i}+\mu,y,\uparrow} - d^{\dagger}_{\mathbf{i},y,\uparrow} d^{\dagger}_{\mathbf{i}+\mu,x,\downarrow} - d^{\dagger}_{\mathbf{i},y,\downarrow} d^{\dagger}_{\mathbf{i}+\mu,x,\uparrow}), \tag{18}$$

or, in momentum space,

$$\Delta^{\dagger}(\mathbf{k})_{\sigma} = (\cos k_x + \cos k_y)(d^{\dagger}_{\mathbf{k},x,\sigma} d^{\dagger}_{-\mathbf{k},y,\sigma} - d^{\dagger}_{\mathbf{k},y,\sigma} d^{\dagger}_{-\mathbf{k},x,\sigma}), \tag{19}$$

$$\Delta^{\dagger}(\mathbf{k})_0 = (\cos k_x + \cos k_y)(d^{\dagger}_{\mathbf{k},x,\uparrow} d^{\dagger}_{-\mathbf{k},y,\downarrow} + d^{\dagger}_{\mathbf{k},x,\downarrow} d^{\dagger}_{-\mathbf{k},y,\uparrow} - d^{\dagger}_{\mathbf{k},y,\uparrow} d^{\dagger}_{-\mathbf{k},x,\downarrow} - d^{\dagger}_{\mathbf{k},y,\downarrow} d^{\dagger}_{-\mathbf{k},x,\uparrow}). \tag{20}$$

This operator is invariant under the A_{2g} irreducible representation of the group D_{4h}, it is odd under orbital exchange, and it is a spin triplet.

However, in our previous effort we have also identified regions of parameter space where the state with two extra electrons is a spin *singlet*, which appears to be compatible with the results of experiments that favor singlet states over triplets.[38,40,90] The dominant pairing operator for the singlet is given by

$$\Delta^{\dagger}(\mathbf{i}) = \sum_{\alpha} d^{\dagger}_{\mathbf{i},\alpha,\uparrow}(d^{\dagger}_{\mathbf{i}+\hat{x},-\alpha,\downarrow} + d^{\dagger}_{\mathbf{i}+\hat{y},-\alpha,\downarrow} + d^{\dagger}_{\mathbf{i}-\hat{x},-\alpha,\downarrow} + d^{\dagger}_{\mathbf{i}-\hat{y},-\alpha,\downarrow}), \tag{21}$$

which in momentum space becomes

$$\Delta^{\dagger}(\mathbf{k}) = \sum_{\alpha} (\cos k_x + \cos k_y) d^{\dagger}_{\mathbf{k},\alpha,\uparrow} d^{\dagger}_{-\mathbf{k},-\alpha,\downarrow}. \tag{22}$$

This operator transforms as the B_{2g} irreducible representation of the D_{4h} point group, it is even under orbital exchange, and it is a spin singlet. As explained in Sec. I, the experimental results favoring spin-singlet pairing lead us to focus our effort on this spin-singlet operator in Secs. IV A–IV C.

IV. EXACT DIAGONALIZATION RESULTS

A. Method

In this section, the Lanczos or exact diagonalization (ED) method will be used to obtain the ground state of the two-orbital model, both at half-filling and also for a system with two electrons more than half-filling. Due to the exponential growth of the Hilbert space with increasing cluster sizes, here our effort must be restricted to a tilted $\sqrt{8} \times \sqrt{8}$ cluster.[76] Using translational invariance, the Hilbert space can be reduced to 21 081 060 states at half-filling and 16 359 200 for two electrons away from half-filling. Taking into account the additional symmetries of spin inversion as well as rotations, the dimension of the Hilbert space becomes $\approx 2\,600\,000$. The employed Lanczos scheme is standard and requires up to 11 Gbytes of memory when only translational invariance is used. Note that the two-orbital eight-site cluster has a similar Hilbert-space size as a 16-site one-band Hubbard lattice, and they are similarly computationally demanding. The focus of our effort is on ground states for a fixed set of quantum numbers corresponding to the symmetries that were implemented. We use both the hoppings from the SK approach and

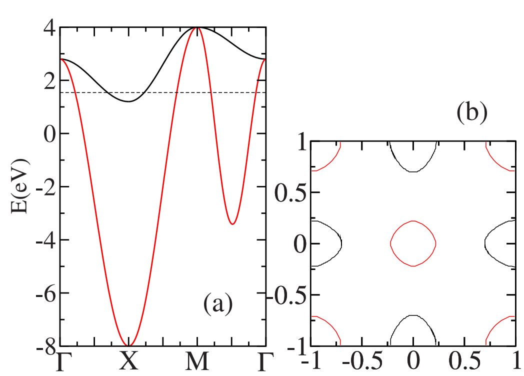

FIG. 8. (Color online) (a) Energy vs momentum for the noninteracting tight-binding Hamiltonian (14) using the hopping amplitudes obtained from fits of band-structure calculations (Ref. 73): $t_1 = -1.0$, $t_2 = 1.3$, and $t_3 = t_4 = -0.85$ (all in eV units). Results are plotted along the path $(0,0)-(\pi,0)-(\pi,\pi)-(0,0)$. (b) Fermi surface for the half-filled system.

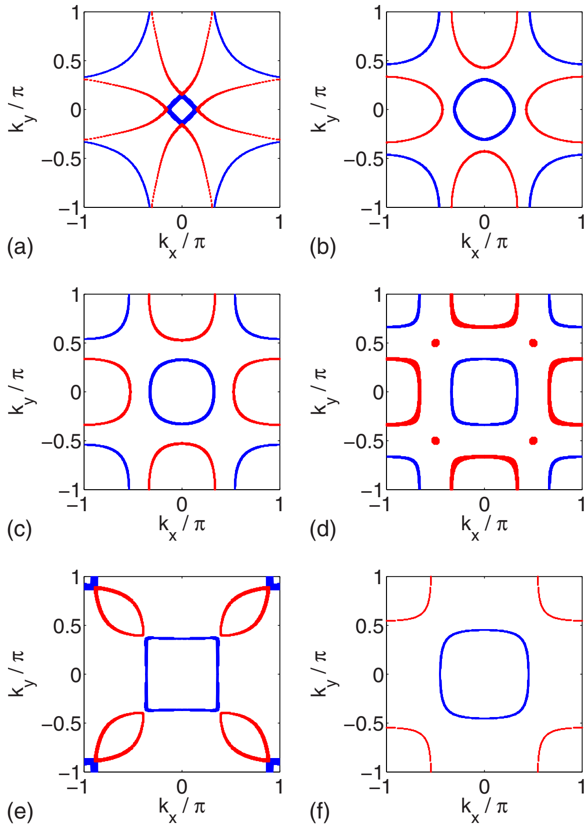

FIG. 9. (Color online) Noninteracting ($U=J=0$) Fermi surface in the unfolded Brillouin zone at the $pd\pi/pd\sigma$s indicated. The realistic regime is $pd\pi/pd\sigma<0$ since hole pockets around (0,0) and (π,π) and electron pockets around $(0,\pi)$ and $(0,\pi)$ are observed.

also the hoppings that fit band-structure calculations and find qualitatively consistent results for both sets.

B. Results using Slater-Koster derived hoppings

1. Fermi surfaces, spin order, and spin of the pairs

In the SK approach, the parameter $pd\sigma$ is here kept fixed equal to 1, providing the scale and the free parameter $pd\pi$ is varied. To constrain the values of $pd\pi$, let us return to the tight-binding Hamiltonian. Figure 9 shows how the Fermi surface evolves by changing $pd\pi$. These figures are in the unfolded Brillouin zone, i.e., for one Fe atom per unit cell. For a negative ratio $pd\pi/pd\sigma$, hole pockets around momenta (0, 0) and (π,π) and electron pockets around $(0,\pi)/(\pi,0)$ are found. However, for a vanishing ratio $pd\pi=0$, additional electron pockets appear at $(\pi/2,\pi/2)$, while the pockets around $(0,\pi)$ and $(\pi,0)$ disappear fast by further increasing $pd\pi$ to positive values. As discussed before,[76] the robust NNN hopping t_3 at negative $pd\pi/pd\sigma$ induces tendencies toward a $(0,\pi)/(\pi,0)$ magnetic ordering at half-filling, as shown by the spin structure factor in Fig. 10(a). This is in good agreement with neutron scattering experiments. Thus, it is clear that the realistic regime corresponds to negative $pd\pi$, and an opposite sign of $pd\pi$ and $pd\sigma$ is also what would be expected from the tabulated values.[95]

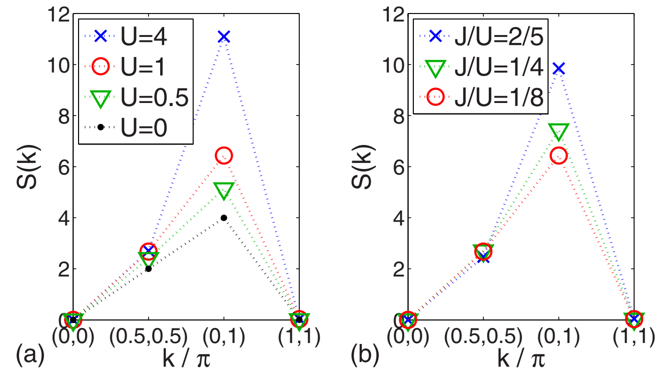

FIG. 10. (Color online) Spin structure factor $S(k)$ at half-filling obtained with ED on a $\sqrt{8}\times\sqrt{8}$ cluster for $pd\pi/pd\sigma=-0.2$. (a) Results corresponding to several U's and $J/U=1/8$. (b) Results varying J at fixed $U=1$.

As it can be observed in Fig. 10(a), the onsite repulsion U enhances the spin "striped" ordering, which is already dominant even at $U=0$ (although in this noninteracting case a power-law decay in the spin correlations is expected rather than genuine long-range order). Increasing Hund's coupling J at a fixed U [see Fig. 10(b)] produces a similar effect because it leads to larger localized moments, allowing for a stronger overall collective spin ordering. However, for positive $pd\pi$, the diagonal hopping t_3 is no longer strong enough to drive the $(\pi,0)$ order, and the spin structure factor peaks at (π,π) instead [Fig. 11(a)]. Figure 11(b) shows the spin structure factor for $pd\pi/pd\sigma=-0.2$, $U=0.5$, and $J=U/8$ when two more electrons are added to half-filling. The $(0,\pi)$ order is weakened in the doped system.

In our previous effort,[76] we investigated the pairing symmetry for two added electrons in the region of hoppings $-0.5\leq pd\pi\leq-0.2$, varying U, and for the special case $J/U=1/4$. The spin of the state with two additional electrons can be determined by comparing the ground state energy for a total z component of the spin $S_z=0$ to $S_z=1$. If these two energies are degenerate, the state is a triplet (it was also tested that the ground state of $S_z=2$ is not degenerate with $S_z=0$ and 1, thus excluding higher spin states). The Hubbard

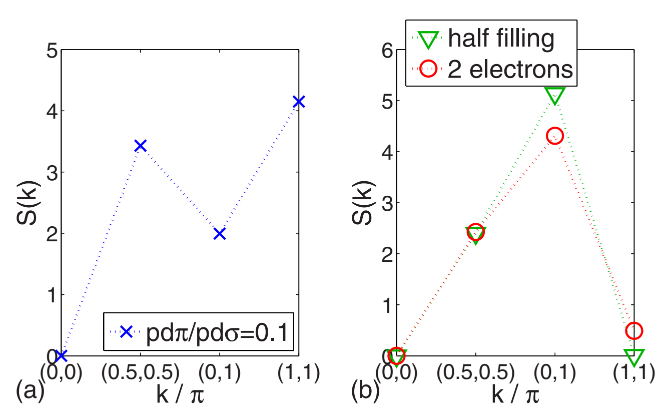

FIG. 11. (Color online) Spin structure factor $S(k)$ for (a) half-filling and $pd\pi/pd\sigma=0.1$, $U=0.5$, $J=U/8$ and (b) $pd\pi/pd\sigma=-0.2$, $U=0.5$, $J=U/8$ at half-filling and with two additional electrons. These are ED results on a $\sqrt{8}\times\sqrt{8}$ cluster.

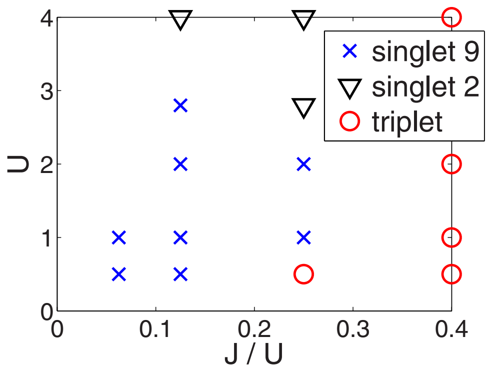

FIG. 12. (Color online) Dominant pairing tendencies of the ground state corresponding to two more electrons than half-filling at $pd\pi=-0.2$. The notations singlet 9 and singlet 2 are explained in the text.

repulsion U was found to drive the spin of the two electrons added to the half-filled system from triplet at small U to singlet at larger U for the $pd\pi$'s investigated. The critical U_c needed for the transition was found to be the lowest at $pd\pi\approx-0.2$. This value of $pd\pi$ moreover leads to a Fermi surface with hole and electron pockets similar to that obtained with band structure after folding [see Ref. 76 and Fig. 9(b)]. For large $|pd\pi/pd\sigma|$, on the other hand, the Fermi surface has far larger electron pockets around $(0,\pi)$ and $(\pi,0)$ than those found in band calculations or experiments [see Fig. 9(a)]. Consequently, we will mainly focus on $pd\pi/pd\sigma=-0.2$ below.

In Fig. 12, the regions where singlet and triplet pairings dominate, depending on U and J, are shown. [The notation "singlet 9" and "singlet 2" refer spin-singlet states with B_{2g} and A_{1g} symmetries, as discussed in more detail in the "pairing symmetry" section below as well as in Eq. (A8).] The trends observed for $J/U=1/4$ remain stable for other realistic values of J. Additionally, qualitatively we have observed that increasing the Hund coupling J promotes a robust triplet pairing. Due to the relation used between U, U', and J, two electrons on the same site, but in different orbitals, no longer feel any Coulomb repulsion for the maximal $J=2U/5$. As a consequence, values of $J/U\gtrsim0.4$ are here considered unphysical.

2. Pairing symmetry

To investigate the symmetry under rotations of the pairing states, the half-filled ground state is compared to states with two additional electrons. The symmetry sector of the half-filled ground state must be contrasted with the symmetry of the doped state, and the symmetry operation leading from one to the other gives us an indication for the pairing symmetry. This method was very successful in establishing the d-wave character of the pairing in the t-J model for the cuprates.[97] In addition, we also added a pair of electrons with a well-defined symmetry under rotations to the half-filled ground state and calculate the overlap between the resulting state and the ground state obtained for half-filling plus two electrons.

From this analysis, we found that the dominant pairing operator for spin-singlet pairs is interorbital and given by[76]

$$\Delta_9^\dagger=\frac{1}{2N_{\text{sites}}}\sum_{\mathbf{i},\alpha,\mu}(d^\dagger_{\mathbf{i},-\alpha,\uparrow}d^\dagger_{\mathbf{i}+\hat{\mu},\alpha,\downarrow}-d^\dagger_{\mathbf{i},\alpha,\downarrow}d^\dagger_{\mathbf{i}+\hat{\mu},-\alpha,\uparrow}),\qquad(23)$$

where $\mathbf{i}=1,\ldots,N_{\text{sites}}$ denotes the lattice site, $\hat{\mu}=\hat{x},\hat{y}$ are the unit vectors connecting NN sites, and $\alpha=x,y$ are the xz and yz orbitals, respectively. This operator transforms as B_{2g}, and it is 9 in the detailed list provided in Ref. 89. In addition to the B_{2g} pairing between nearest-neighbor sites, we also find a small overlap for the corresponding B_{2g} onsite pairing 8 (reaching at most 10% of the intersite overlap) and some overlap for the NNN B_{2g} pairing. In contrast to the small onsite contribution, the NNN pairing is sizable, but its exact strength compared to NN pairing is difficult to ascertain with the small cluster used.

The only other singlet pairing for which we have found a substantial overlap is 2 in the above mentioned list, although, as discussed below, its region of stability at large U does not have the correct properties expected for the FeAs superconductors. This operator is intraorbital has A_{1g} symmetry, and it is given by

$$\Delta_2^\dagger=\frac{1}{2N_{\text{sites}}}\sum_{\mathbf{i},\alpha,\mu}(d^\dagger_{\mathbf{i},\alpha,\uparrow}d^\dagger_{\mathbf{i}+\hat{\mu},\alpha,\downarrow}-d^\dagger_{\mathbf{i},\alpha,\downarrow}d^\dagger_{\mathbf{i}+\hat{\mu},\alpha,\uparrow}).\qquad(24)$$

Applying the pairing operators $\Delta_i^\dagger$ to the half-filled ground state $|\phi_0\rangle$, we find that the resulting vector $\Delta_i^\dagger|\phi_0\rangle$ has a very small norm $\lesssim0.15$ for pairings $i=3$, 4, 5, and 6 in the list of Ref. 89, while it reaches $\approx0.6-0.8$ (depending on U and J) for 1, 2, 7, 8, and 9. Then, at least qualitatively, we conclude that only the latter pairs can be created easily in the half-filled ground state. To provide more quantitative information, we then calculate the overlap between $\Delta_i^\dagger|\phi_0\rangle$ and the ground state found for half-filling plus two additional electrons $|\phi_2\rangle$. We only find substantial overlaps for the operators 9 (B_{2g}) and 2 (A_{1g}) given in Eqs. (23) and (24), while $\Delta_7^\dagger|\phi_0\rangle$ is always orthogonal to the two-electron ground state $|\phi_2\rangle$, at least for the range of parameters investigated. As it can be observed in Fig. 13, the B_{2g} pairing Eq. (23) occurs at small to intermediate Coulomb repulsion U, which is the expected suitable regime to describe noninsulating materials with bad metallic properties. Only for large $U\gtrsim2.8$ eV, where a hard gap in the density of states indicates insulating behavior,[76] we do find the pairing [Eq. (24)] with A_{1g} symmetry. In this regime we find some admixture of the corresponding onsite pairing (1) and the longer-range A_{1g} NNN pairing which, as shown in Eq. (A8), corresponds to the much discussed $s\pm$ pairing state.[49,61,62,65]

Figure 12 shows more explicitly the regions of dominance of the states 9 (B_{2g}) and 2 (A_{1g}) in the U vs J/U plane. Thus, the B_{2g} symmetric operator seems to be the most realistic in the regime $pd\pi/pd\sigma\approx-0.2$ and $0.5\lesssim U\lesssim1$, which is the appropriate region of parameters to qualitatively describe the FeAs-based superconductors.[98]

C. Results with hopping parameters fitted to band-structure calculations

1. Results at nonzero J

We have also investigated the two-orbital model using hopping parameters obtained from a fit to band-structure cal-

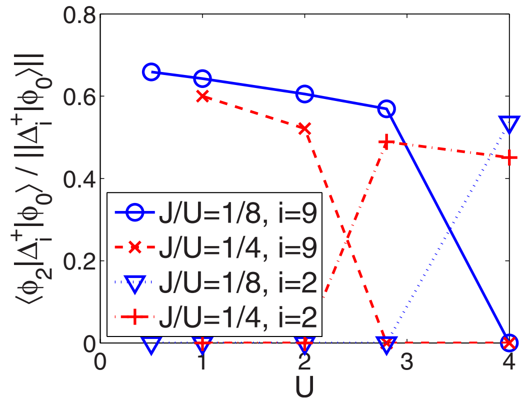

FIG. 13. (Color online) Overlap between the ground state for half-filling plus two electrons $|\phi_2\rangle$ and the state obtained by applying the pairing operators $\Delta_2^\dagger$ and $\Delta_9^\dagger$ to the undoped ground state $|\phi_0\rangle$. At small to intermediate U, the interorbital singlet pairing operator $\Delta_9^\dagger$ with B_{2g} symmetry ($i=9$) dominates [see Eq. (23)]. For large U, the intraorbital singlet $\Delta_2^\dagger(i=2)$ dominates. Results were obtained using $pd\pi/pd\sigma=-0.2$ and the ED technique on $\sqrt{8}\times\sqrt{8}$ site clusters.

culation results.[73] It is interesting to observe that this set of parameters also leads to $(0,\pi)/(\pi,0)$ antiferromagnetic order at half-filling (see Fig. 14), which is again enhanced by increasing U at fixed J or increasing J at fixed U. As for SK hoppings, Fig. 15 shows that the magnetic order is only slightly reduced by the doping with two electrons. In Fig. 16, we report the spin of the state with two electrons added to the half-filled state and find qualitatively similar behavior as with the SK approach: U promotes singlet pairing, in the previously discussed "9" (B_{2g}) and "2" (A_{1g}) channels, and J favors triplet pairing.

We have performed an analogous analysis of the electron pairing as in Sec. IV B 2 and again find the interorbital singlet operator [Eq. (23)] to dominate at intermediate U and J. Table III gives the pairing amplitudes for operators [Eqs. (23) and (24)] for several (U,J) parameter sets. As before, the Coulombic parameters were chosen to give a spin-singlet state for two electrons added to half-filling but are expected

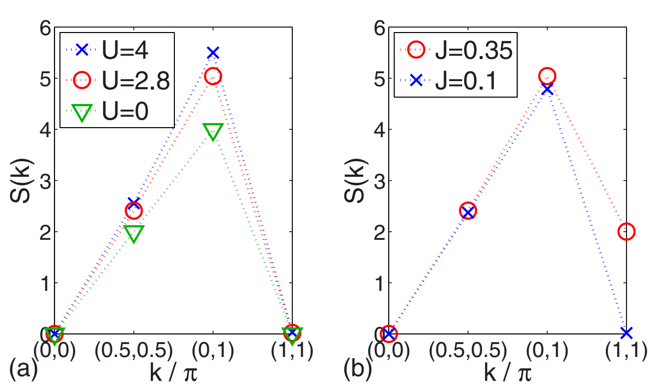

FIG. 14. (Color online) Spin structure factor $S(k)$ for hopping parameters $t_1=-1.0$, $t_2=1.3$, $t_3=t_4=-0.85$ (in eV units) (Ref. 73): (a) results for several values of U and $J/U=1/8$; (b) results for two values of J, with $U=2.8$ eV fixed. (a) and (b) were obtained at half-filling using ED on $\sqrt{8}\times\sqrt{8}$ clusters.

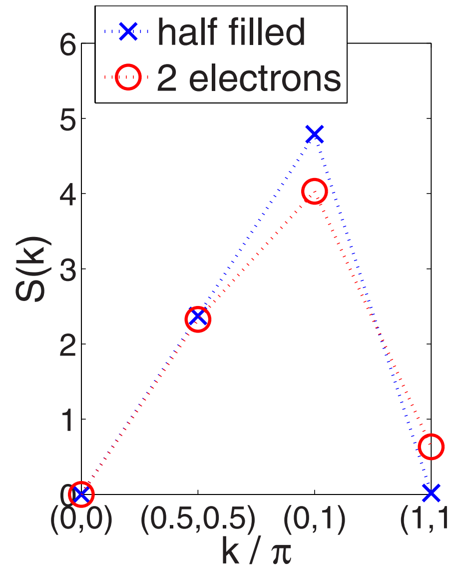

FIG. 15. (Color online) Spin structure factor $S(k)$ for half-filling and half-filling plus two electrons, using the hopping parameters $t_1=-1.0$, $t_2=1.3$, $t_3=t_4=-0.85$ (Ref. 73), and $U=2.8$, $J=0.1$ (in eV units). These are ED results for $\sqrt{8}\times\sqrt{8}$ clusters.

to be small enough to remain in the metallic regime. As for SK hoppings, the pairing symmetry for these singlet states is B_{2g}, i.e., the interorbital singlet Eq. (23) dominates here as well.

Interorbital pairing is favored over intraorbital pairing by the kinetic energy because the interorbital Coulomb repulsion U' is weaker than the repulsion U within the orbitals. To test this assumption, we analyze pairing amplitudes for the special case $J=0$ but instead of using $U=U'$, we use $U' < U$, i.e., we deviate from the relation $U'=U-2J$. The resulting pairing symmetry is still the same B_{2g} interorbital singlet [Eq. (23)], as deduced from the amplitudes in Table IV.

2. Results at $J=0$ and $U=U'$

Finally, let us discuss the special case $J=0$, $U=U'$ for $U=2.8$ (in eV units), which are the couplings used in Ref. 73. In contrast to $J \gtrsim 0.05$ and $U' \lesssim 2.6$, we here find that the

TABLE III. Overlap between the ground state $|\phi_2\rangle$ for two electrons added to half-filling and the states $\Delta_i^\dagger|\phi_0\rangle$ that are obtained by applying pairing operators [Eqs. (23) and (24)] to the ground state at half-filling. Data are for a kinetic-energy operator obtained from band-structure fitting with $t_1=-1.0$, $t_2=1.3$, and $t_3=t_4=-0.85$ (in eV units) (Ref. 73).

U	J	$\langle\phi_2\|\Delta_2^\dagger\|\phi_0\rangle$	$\langle\phi_2\|\Delta_9^\dagger\|\phi_0\rangle$
1.4	0.10	0.00	0.64
2.8	0.00	0.66	0.00
2.8	0.05	0.00	0.66
2.8	0.10	0.00	0.66
4.0	0.50	0.00	0.65
10.0	1.25	0.58	0.00

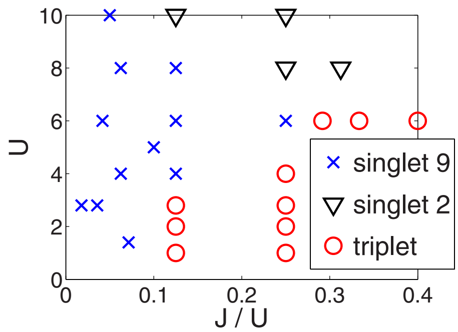

FIG. 16. (Color online) Dominant pairing tendencies of the ground state for two more electrons than half-filling, with hoppings fitted to band-structure results.(Ref. 73). The singlet 9 and singlet 2 notations are the same as for the case of the Slater-Koster hoppings.

A_{1g} intraorbital singlet [Eq. (24)] has the lowest energy, i.e., the same pairing as observed at large U for both the fitted and the SK hoppings. However, at $U=U'=2.8$ and $J=0$, the second lowest eigenstate is almost degenerate with the ground state, and it gives an overlap with Eq. (23), i.e., pairing 9. The third state at these couplings corresponds to the intraorbital pairing 7 (B_{1g}). Table V contains the explicit numbers for energies and overlaps. The near degeneracy of these states does not allow us to reach a clear conclusion for the $J=0$ and $U=U'$ case, which appears to be singular, since small modifications away from our results, such as increasing lattice sizes, may change the relative order of the competing states.

3. Competing magnetic states at half-filling

The magnetic phase diagram for the present model was also studied using a mean-field approximation.[80] At half-filling, it was claimed that the Coulomb repulsion rather than stabilizing a state with $(\pi,0)/(0,\pi)$ spin-stripe order induces an "orthomagnetic" (OM) ordering where NN spins are at right angles. The spin structure factor for this phase is still peaked at $(0,\pi)$ and $(\pi,0)$. We have tried to address this issue with the ED technique on the eight-site cluster. Unfortunately, several observables are expected to give similar results for the two states. Apart from having similar spin structure factors, diagonal NNN spin-spin correlations are also negative in both states. Moreover, the expectation value for NN correlations vanishes in both cases: in the OM state the NN spins are at 90°, while in the stripe state the cancellation occurs because the small cluster ground state $|\phi_0\rangle$ contains both $(0,\pi)$ and $(\pi,0)$ configurations with equal weight and NN correlations $\langle\phi_0|v_x\rangle$ and $\langle\phi_0|v_y\rangle$ average out, where

TABLE IV. Overlap $\langle\phi_2|\Delta_i^\dagger|\phi_0\rangle$ as in Table III, but with $J=0$. The coupling U' is different from U, and the hoppings were $t_1=-1.0$, $t_2=1.3$, and $t_3=t_4=-0.85$ (in eV units).

U	U'	$\langle\phi_2\|\Delta_2^\dagger\|\phi_0\rangle$	$\langle\phi_2\|\Delta_9^\dagger\|\phi_0\rangle$
2.8	2.8	0.66	0
2.8	2.6	0	0.66
2.8	1.4	0	0.62

TABLE V. Energy of the lowest eigenstates for two electrons and $J=0$, $U=U'=2.8$, and pairing operators giving the largest overlap when applied to the half-filled state. Hoppings are those from band-structure fitting.

	Energy	Pairing No.	$\langle\phi_2\|\Delta_i^\dagger\|\phi_0\rangle$
1	−8.45322	2	0.66
2	−8.45150	9	0.66
3	−8.4132	7	0.67

$$|v_x\rangle = \frac{1}{N_{\text{sites}}}\sum_{\mathbf{i}} \mathbf{S_i}\cdot\mathbf{S}_{\mathbf{i}+\hat{x}}|\phi_0\rangle, \tag{25}$$

$$|v_y\rangle = \frac{1}{N_{\text{sites}}}\sum_{\mathbf{i}} \mathbf{S_i}\cdot\mathbf{S}_{\mathbf{i}+\hat{y}}|\phi_0\rangle. \tag{26}$$

Our numerical ED results indeed give very small negative values for the NN spin correlation. However, we expect the two states to lead to different results for $\langle v_x|v_x\rangle$ and $\langle v_y|v_x\rangle$: $\langle v_x|v_x\rangle$ is expected to be positive and $\langle v_y|v_x\rangle$ to be negative in the spin-striped phase, while both should be zero or very small in the OM phase. Table VI shows the results for strong ($U=4$), intermediate ($U=1$), and weak ($U=0.5$) on-site Hubbard repulsions. For $U=4$, we clearly find $\langle v_y|v_x\rangle<0$ and $\langle v_x|v_x\rangle>0$. While these numbers become weaker for the less spin ordered states at smaller U, they are still consistent with the $(0,\pi)/(\pi,0)$ ordering. For comparison, we also include results obtained for a linear combination of states with perfect Ising-type $(0,\pi)$ and $(\pi,0)$ orders in the z direction. These results are useful to judge the expected order-of-magnitude values for the correlations investigated. The numbers on Table VI show that the numerical results for the two-orbital model are compatible with those of the Ising spin-stripe state, particularly considering that quantum fluctuations will reduce the spin correlations of such a state. As a consequence, our present investigations favor the spin-stripe magnetic state, although further work is needed to fully confirm these conclusions.

V. DISCUSSION OF NODAL STRUCTURE IN THE MEAN-FIELD APPROXIMATION

In this section, the results of a pairing mean-field analysis of the two-orbital Hamiltonian will be discussed. The nu-

TABLE VI. Four-spin correlations $\langle v_x|v_x\rangle$ and $\langle v_y|v_x\rangle$ for two parameter sets using the full two-orbital model at the values of U and J indicated, on an eight-site cluster. For comparison, results using a perfect Ising-type $(0,\pi)+(\pi,0)$ state on eight sites are also shown.

	Ising	$U=4$ $J=1$	$U=1$ $J=0.25$	$U=0.5$ $J=0.0625$
$\langle v_y\|v_x\rangle$	−1	−0.64	−0.1684	−0.07776
$\langle v_x\|v_x\rangle$	0.0625	0.02735	0.02856	0.0225

merical results of Secs. I–IV and experimental data will be used to guide this mean-field approximation. Experiments indicate that the pairs in the Fe-based superconductors are spin singlets[38,40,90] and our previous numerical results did provide a dominant spin-singlet pairing operator, as discussed in Sec. IV C 3. It is also important to note that the pairing operator that we obtained mixes different orbitals. A numerical study of the orbital composition of the bands that determine the FS in our two-orbital model indicates that the bands that constitute the pockets are an admixture of xz and yz orbitals. Thus, it is not surprising that the dominant pairing operator creates pairs made of electrons in different orbitals. One of the main goals of the analysis discussed below will be to find out the nodal structure of the mean-field Hamiltonian.

A. Location of the nodes

1. Reminder of one-band model results

For the simple case of d-wave superconductivity in a single-orbital model, characterized by the dispersion relation $\xi(\mathbf{k})=-2t(\cos k_x+\cos k_y)-4t' \cos k_x \cos k_y-\mu$, the gap function is given by $\Delta_k=\Delta(\cos k_x-\cos k_y)$. In this case, the mean-field Hamiltonian reduces to a 2×2 matrix linking $\mathbf{k}$ with $-\mathbf{k}$ which is simply given by

$$H_{\mathrm{MF}}=\begin{pmatrix} \xi(\mathbf{k}) & \Delta_k \\ \Delta_k & -\xi(\mathbf{k}) \end{pmatrix}. \tag{27}$$

To obtain the position of the nodes in the gap, we merely need to find the values of k_x and k_y where the eigenvalues of the matrix [Eq. (27)] are zero. These are the same values that solve the equation $\det(H_{\mathrm{MF}})=0$, i.e., $\xi(\mathbf{k})^2+\Delta_k^2=0$, which is satisfied only if each term vanishes independently. This occurs at the points where the noninteracting Fermi surface described by $\xi(\mathbf{k})=0$ intersects the diagonal lines along which $\Delta_k=0$, i.e., $k_x=k_y$ and $k_x=-k_y$. This procedure establishes the well-known location of the four d-wave nodes of a single-band model.

2. Nodes in a two-orbital model

For a system with two orbitals, we will proceed in an analogous manner as for one orbital. The MF Hamiltonian matrix in the basis $(d^{\dagger}_{\mathbf{k},x,\uparrow},d^{\dagger}_{\mathbf{k},y,\uparrow},d_{-\mathbf{k},x,\downarrow},d_{-\mathbf{k},y,\downarrow})$ is now given by the 4×4 matrix,

$$H_{\mathrm{MF}}=\begin{pmatrix} \xi_{xx} & \xi_{xy} & 0 & \Delta_k \\ \xi_{xy} & \xi_{yy} & \Delta_k & 0 \\ 0 & \Delta_k & -\xi_{xx} & -\xi_{xy} \\ \Delta_k & 0 & -\xi_{xy} & -\xi_{yy} \end{pmatrix}. \tag{28}$$

The matrix elements can be obtained by Fourier transforming the tight-binding Hamiltonian H_{TB} given in Eq. (14). We obtain

$$\xi_{xx}=-2t_2 \cos k_x-2t_1 \cos k_y-4t_3 \cos k_x \cos k_y-\mu,$$

$$\xi_{yy}=-2t_1 \cos k_x-2t_2 \cos k_y-4t_3 \cos k_x \cos k_y-\mu,$$

$$\xi_{xy}=-4t_4 \sin k_x \sin k_y, \tag{29}$$

and

$$\Delta_k=V(\cos k_x+\cos k_y), \tag{30}$$

where V is the strength of the pairing interaction.

Note that we can also work in the basis in which H_{TB} is diagonal. In this basis, which is expanded by $(c^{\dagger}_{k,1,\uparrow},c^{\dagger}_{k,2,\uparrow},c_{-k,2,\downarrow},c_{-k,1,\downarrow})$, H_{MF} becomes $H'_{\mathrm{MF}}=U^{-1}H_{\mathrm{MF}}U$ given by

$$H'_{\mathrm{MF}}=\begin{pmatrix} \epsilon_1 & 0 & V_{\mathrm{B}} & V_{\mathrm{A}} \\ 0 & \epsilon_2 & -V_{\mathrm{A}} & V_{\mathrm{B}} \\ V_{\mathrm{B}} & -V_{\mathrm{A}} & -\epsilon_2 & 0 \\ V_{\mathrm{A}} & V_{\mathrm{B}} & 0 & -\epsilon_1 \end{pmatrix}, \tag{31}$$

where V_{A} and V_{B} are given by

$$V_{\mathrm{A}}=2uv\Delta_k, \tag{32}$$

$$V_{\mathrm{B}}=(v^2-u^2)\Delta_k, \tag{33}$$

and u and v are the elements of the change of basis matrix U given by

$$U=\begin{pmatrix} u & v & 0 & 0 \\ v & -u & 0 & 0 \\ 0 & 0 & v & u \\ 0 & 0 & -u & v \end{pmatrix}, \tag{34}$$

with $U^{-1}=U^T$. Remember that V_{A}, V_{B}, u, and v are all functions of the momentum k and $u^2+v^2=1$.

Now let us discuss the physical meaning of V_{A} and V_{B}. According to Eq. (31), V_{A} is the intraband pairing for band 1, i.e., the band with the highest energy (electron band), while the intraband pairing for band 2 (hole band) is $-V_{\mathrm{A}}$. Thus, there is a relative phase π between the two intraband order parameters. In the standard BCS studies for multiband models, it is expected that pairs are formed by electrons in the same band.[92] In the two-orbital model, as just discussed, we found intraband pairing but we also obtain *interband pairing* with strength V_{B}. The possibility of interband pairing has been considered previously in several contexts: (i) possibility of T_c,[99] (ii) high T_c cuprates,[100] and (iii) heavy fermion systems,[101] where it was shown that if two bands are very close to each other in the vicinity of the Fermi level, interband pairing can occur. The weaker the pairing potential, the closer to the Fermi surface the two bands have to be. When long-range pairing develops the Brillouin zone gets folded and, as a result, the total number of bands doubles. In this representation, which arises by diagonalizing Eq. (28) with $\Delta_k=0$, the two-orbital model has the dispersion shown in Fig. 17 where each band [panel (a)] and FS [panel (b)] is represented with a different color and the folded (unfolded) portions with dashed (continuous) lines. It can be seen from panel (a) that at the Fermi level there is only intraband crossing indicated by circles. However, there is also interband crossing, indicated by the boxes, above the Fermi energy. The previous numerical results appear to indicate that the effective coupling is sufficiently strong as to produce inter-

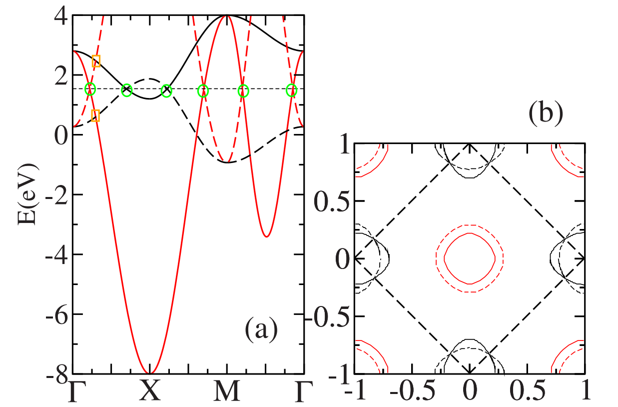

FIG. 17. (Color online) (a) Energy vs momentum for the noninteracting tight-binding Hamiltonian (14) using the hoppings from band-structure calculations (Ref. 73), $t_1=-1$, $t_2=1.3$, and $t_3=t_4=-0.85$ (in eV units). These noninteracting results are shown as continuous lines. Also shown are the additional Bogoliubov bands produced by the pairing interaction considered in this work (dashed lines). The circles (boxes) indicate the bands that contribute electrons to the intraband (interband) pairs at different locations close to the FS (for a discussion see text). (b) Fermi surface for the corresponding noninteracting half-filled system.

band pairing. In Fig. 18 it can be seen that even a small V opens a gap between the two bands that cross away from the FS. In multiorbital models the opening of these gaps can lower the overall energy.[102] Within the standard BCS approach this result may appear counterintuitive and it could be an artifact of the two-orbital model or of the small system size that we have considered. However, there are clear indications that most of the FSs in the five-orbital model have characters d_{xz} and d_{yz} (Refs. 60 and 91) and, in such a case, the only possible pairing operators that respect the symmetry

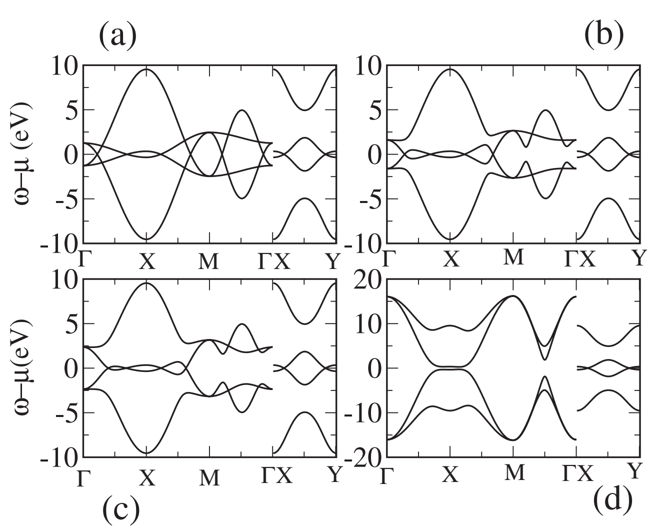

FIG. 18. (a) Energy vs momentum for the mean-field Hamiltonian using $t_1=-1$, $t_2=1.3$, and $t_3=t_4=-0.85$ (in eV units) (Ref. 73). The Bogoliubov bands produced by the pairing interaction considered in this work are also shown, with equal intensity. The four panels correspond to four different values of the pairing attraction: (a) $V=0$, (b) $V=0.5$, (c) $V=1$, and (d) $V=8$.

of the FeAs planes are those that have been considered in our calculations and others.[89] In fact, none of the 16 pairing operators that combine these two orbitals leads to a purely intraband pairing interaction. This, of course, could be an indication that other orbitals have to participate in the model but we believe that it is still instructive to consider the nodal structure that results from the pairing operator that was favored numerically within the two-orbital model and attempt to compare the results with experiments.

The existence and position of nodes in the resulting mean-field band structure can be found by requesting that $\det(H'_{\rm MF})=0$, as in the one-orbital case. From Eq. (31), we obtain the following equation:

$$V_{\rm A}^2(V_{\rm A}^2+2V_{\rm B}^2+\epsilon_1^2+\epsilon_2^2)+(\epsilon_1\epsilon_2+V_{\rm B}^2)^2=0. \qquad (35)$$

This equation is satisfied in two possible ways:

(1) First, a solution can be found if $V_{\rm A}=V_{\rm B}=0$, and $\epsilon_1=0$ or $\epsilon_2=0$. Thus, this condition for nodes is satisfied if the lines where $\cos k_x+\cos k_y=0$, namely, the lines where $V_{\rm A}$ and $V_{\rm B}$ vanish, intersect any of the noninteracting Fermi surfaces determined by the points where $\epsilon_1=0$ or $\epsilon_2=0$. It is clear that the line $\cos k_x+\cos k_y=0$ intersects each of the four electron-pocket Fermi surfaces in two points per pocket [see Figs. 1(e) and 17(b)]. This means that nodes will appear only in the electron pockets and not in the hole pockets. These are the nodes that arise from a simple extrapolation of the reasoning used to find nodes in the one-orbital model, namely, by finding the intersections of the noninteracting Fermi surface with the trigonometric function, in this case $\cos k_x+\cos k_y$, contained in the Δ_k gap function. The position of the nodes in the electron pockets upon folding of the Brillouin zone [see Figs. 1(d) and 17(b)] is at the points in k space where the two-electron pockets intersect each other.

Note that the existence of these nodes does not depend on the value of V. They will always be present as it can be seen in Fig. 18 where the nodes along the $X-Y$ direction appear in all the panels varying V.

(2) However, the two-orbital nature of this problem leads to the possibility of additional nodes in unexpected locations. This can be understood by realizing that Eq. (35) can also be satisfied if $V_{\rm A}=0$ and

$$V_{\rm B}^2=-\epsilon_1\epsilon_2. \qquad (36)$$

According to the expression for $V_{\rm A}$ in Eq. (32), and assuming that Δ_k is nonzero [if it is zero we recover the nodes already described in (1) above], then the condition $V_{\rm A}=0$ is satisfied if $u=0$ or $v=0$. Due to the normalization $u^2+v^2=1$, when $u=0$ then it must occur that $v=1$ and vice versa. Introducing these values of u and v in Eq. (34), it can be shown that the condition that $H'_{\rm MF}=U^{-1}H_{\rm MF}{\rm U}$ is diagonal is satisfied only if $\xi_{xy}=0$. According to Eq. (29), for ξ_{xy} to vanish it is necessary to have $k_x=0$ or π or $k_y=0$ or π. Then, additional nodes could be expected along these horizontal or vertical lines in the Brillouin zone. Since the product of the two energies $\epsilon_1\epsilon_2$ has to be negative [i.e., the energies cannot vanish, otherwise we recover (1)], the nodes, if they exist, will appear *in between* the hole and electron pockets at locations in k space that *do not* belong to the original tight-binding Fermi surface. To understand this interesting result, consider the ex-

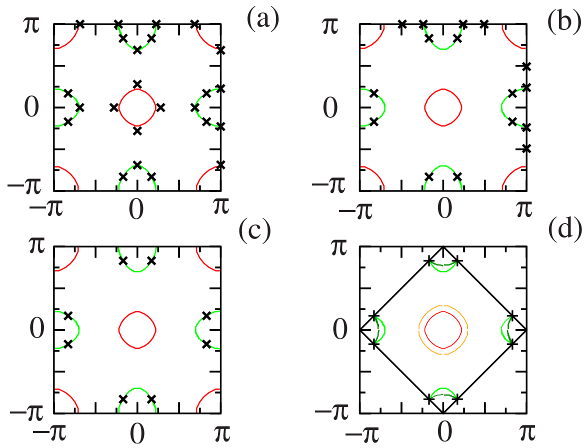

FIG. 19. (Color online) Examples showing the positions of the nodes for the two-orbital model, using the standard pairing mean-field approximation. With solid lines are shown the hole pockets (red) and electrons pockets (green), namely, the Fermi surface in the noninteracting limit $V=0$. The black crosses are the nodes. As example, we use the case of the hopping amplitudes derived from fits with band-structure calculations (Ref. 73). (a) corresponds to the "weak" pairing regime, $V=0.5$, showing the existence of many nodes, both at the electron pockets as well as near the hole pockets. (b) is the example of $V=2.0$ where the number of nodes has been reduced compared with (a). (c) is the "intermediate" $V=3.5$ regime (V is still substantially smaller than the bandwidth) that provides the smaller number of nodes (a total of 8), all being located at the noninteracting electron pockets. (d) is the folded Fermi surface corresponding to case (c) for better comparison with experiments and band calculations.

ample of $k_x=0$. For this special case we obtain

$$V_B^2 = V^2(1+\cos k_y)^2,$$

$$\epsilon_1 = -2t_2 - 2t_1 \cos k_y - 4t_3 \cos k_y - \mu,$$

$$\epsilon_2 = -2t_1 - 2t_2 \cos k_y - 4t_3 \cos k_y - \mu. \qquad (37)$$

Replacing Eq. (37) in Eq. (36), a quadratic equation is obtained that allows us to find the values of $\cos k_y$ where nodes should appear. Depending on the specific values of V, the hopping amplitudes, and μ, the quadratic equation can have two solutions (meaning that two nodes appear along the $k_x=0$ axis between the hole and electron pockets), one solution (meaning just one node), or no solution at all (indicating no extra nodes). Thus, once the folding and rotation of the FBZ is performed, nodes can appear along the diagonals of the BZ in Fig. 1(c) for particular values of the parameter in the model.[103]

A variety of examples obtained numerically illustrates this nontrivial nodal structure, as shown in Fig. 19: (a) at weak V, several nodes are found either at or close to both the hole and electron pockets. In view of recent photoemission experiments reporting the absence of nodes at the hole pockets (see discussion below), this regime is unlikely to be realized experimentally. (b) is obtained increasing V: in this case the number of nodes has decreased. In addition to those coming from solution (1) in the previous discussion, all at the electron pockets, still solution (2) provides some nodes at the boundaries of the Brillouin zone in this regime. (c) is the most canonical result, obtained at intermediate V, with the nodes only appearing in the electron pockets where $\cos k_x + \cos k_y = 0$ intersects the original Fermi surface. Both in (b) and (c) there are no nodes in the Γ centered hole pocket even for this B_{2g} state. (d) provides the results of (c) but in the folded zone for comparison with experiments.

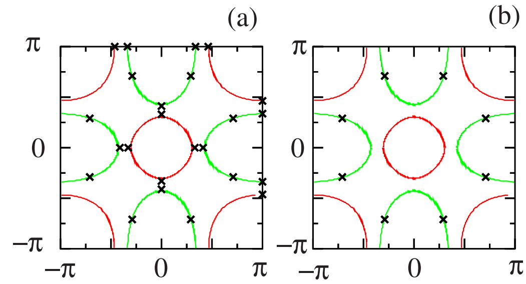

FIG. 20. (Color online) Nodal structure for SK hoppings with $(pd\pi)=-0.2$. (a) is in the weak coupling regime, $V=0.05$, and shows many nodes as in Figs. 19(a) and 19(b). (b) is the intermediate coupling regime, $V=0.5$, where the number of nodes is the minimal (8), similarly as in Figs. 19(c) and 19(d).

Band dispersions obtained with mean-field results are also shown in Fig. 18. We observe how the nodes along the $\Gamma-X$ and $X-M$ directions get closer to each other as V increases from 0 to 0.5 and to 1 and how they have disappeared for $V=8$. It is also interesting to see how the crossing of different bands, indicated by the orange squared boxes in Fig. 17(a), is replaced by a gap as soon as V is finite [see panel (b) in Fig. 18] which appears to be the effect of the interband interaction.

For completeness, in Fig. 20 we provide the nodal structure for the case of hoppings obtained from the Slater-Koster approximation, which gives large pockets in the band-structure calculations. In the weak coupling case, (a), once again several nodes are obtained. This regime appears unrealistic. Increasing V, panel (b) shows that the nodes only remain in the electron pockets, as found before in Figs. 19(c) and 19(d).

In addition to the analytic discussion, we have also searched numerically, using a large lattice 200×200 in k-space, for the zero eigenvalues of the original matrix [Eq. (28)]. These numerical results are in excellent agreement with the analytic discussion, thus showing that the nodal structure of the two-orbital mean-field pairing Hamiltonian has been properly obtained.

3. Comparison with ARPES experiments

How do these theoretical calculations based on the two-orbital model compare with angle-resolved photoemission experiments for the Fe pnictides? In Ref. 45, ARPES results were presented with the focus of the effort on the hole pockets at Γ. It was concluded that nodes were not observed in those hole pockets. This result is compatible with our B_{2g} state since nodes do not appear on the hole pockets, but instead on the electron pockets, at least at intermediate values of the attraction V. In Ref. 46, a similar conclusion was reached but in this case the electron pockets were also studied. However, in that effort the 122 materials for which the FS depends on k_z were analyzed, and only a few cuts in momentum-space were investigated. Recent ARPES experiments that suggest a short Cooper-pair size[104] would suggest that the regime of large V in our study of the nodal structure is the most realistic, thus clearly locating all the nodes in the electron pockets. Then, a more detailed ARPES analysis would be needed to fully conclude that there are no nodes in this system, particularly in the electron pockets.[105] Other recent ARPES experiments have shown a variety of interesting aspects, such as substantial differences with band-structure calculations,[106] which also need to be incorporated in future theoretical studies.

The information provided in this paper for the actual location of the nodes for the B_{2g} state will help to guide future ARPES experiments. In view of the several other experimental investigations that have reported nodes in the Fe-based superconductors,[33–43] we believe this issue is still open and needs further research to arrive to a final conclusion. If future experimental work clearly proves that there are no nodes in the Fe-based superconductors, not only in the hole pockets but more importantly in the electron pockets, then it will be concluded that the two-orbital model used here will not be sufficient to properly describe this family of materials and more orbitals will be needed.[107]

VI. CONCLUSIONS

In this paper, we have studied some properties of a two-orbital approach for the Fe-based superconductors. It is important to find out the minimal model capable of reproducing the basic physics of these materials. By studying a relatively simple model, considerable insight could be reached on the inner mechanisms that cause magnetism and superconductivity in these compounds. While models with more than two orbitals would certainly be more accurate, the difficulty in extracting reliable numbers from the models grows fast with the number of orbitals. Two-orbital models are the minimal that allow for a study of simple multiband effects on magnetism and superconductivity, and also allow for the possibility of exploring orbital order in the pnictide materials[108] in future works.

Here we have shown that the magnetic properties of the undoped parent compound are properly reproduced by a simple two-orbital model: spin stripes are obtained in agreement with neutron scattering experiments. Regarding electron doping, here we follow the same approach as for the cuprates: it is expected that the pairing channel will be unveiled by simply studying the symmetry properties of the state of two electrons added to the half-filled ground state. This approach worked for the models for Cu-oxide superconductors, leading to the d-wave state prediction. Within this assumption, the spin-singlet pairing state that dominates in the phase diagram at realistic values of the Hubbard repulsion U is found to transform according to the B_{2g} representation of the lattice symmetry group. At large Coulomb repulsion U, too large to describe the metallic state of the undoped compound, we found that the relative symmetry of the undoped and electron doped ground states is the same and, thus, they are connected by a pairing operator that transforms according to A_{1g}. We showed that the NNN pairing operator with this symmetry is the $s\pm$ state and that this state, according to our numerical calculations, prevails only in an unphysical regime of parameters. On the other hand, for a robust electron-electron effective attraction to form Cooper pairs, assumption compatible with the conclusions of recent ARPES experiments, the B_{2g} pairing state found for realistic U has nodes only in the electron pockets. All our main conclusions do not depend qualitatively on the set of hopping amplitudes used: our results appear to be representative of the two-orbital framework in general and not merely of a particular model with particular couplings. Thus, a conclusion of our study is that more refined ARPES experiments in the superconducting state are needed to analyze the possible existence of nodes in the electron pockets. These future experiments will provide crucial information to guide the theoretical search for the minimal model that captures the physics of the Fe pnictides.

ACKNOWLEDGMENTS

The authors thank E. Arrigoni and D. Scalapino for useful discussions. This work was supported by the NSF under Grant No. DMR-0706020 and the Division of Materials Science and Engineering, U.S. DOE, under contract with UT-Battelle, LLC.

APPENDIX A: EFFECTIVE INTERACTION THAT GENERATES THE B_{2g} PAIRING OPERATOR

The mean-field superconducting state discussed before could originate from an effective attractive density-density interaction dynamically generated in the original Hamiltonian or induced by particular phononic modes if an electron-phonon coupling is incorporated. The form of this attraction is

$$H_{\rm attr} = -V \sum_{\mathbf{i},\mu,\alpha,\sigma} n_{\mathbf{i},\alpha,\sigma} n_{\mathbf{i}+\mu,-\alpha,-\sigma}, \tag{A1}$$

and below we prove that indeed it generates the correct pairing term. It is well-known that a similar nearest-neighbor density-density attraction of the form $-Vn_{\mathbf{i}}n_{\mathbf{i}+\mu}$ leads to d-wave superconductivity in a mean-field treatment of the one-band repulsive U Hubbard model,[109] and here we merely generalize this concept to two orbitals.

Let us discuss the mean-field treatment of $H_{\rm attr}$. In momentum space, the Fourier transformed of this effective attraction is

$$H_{\rm attr} = -\sum_{\mathbf{k},\mathbf{k}',\alpha,\sigma} V_{\mathbf{k},\mathbf{k}'} d^{\dagger}_{\mathbf{k},\alpha,\sigma} d^{\dagger}_{-\mathbf{k},-\alpha,-\sigma} d_{-\mathbf{k}',-\alpha,-\sigma} d_{\mathbf{k}',\alpha,\sigma}, \tag{A2}$$

where we have requested that the pairing occurs between electrons with opposite momentum (thus, we have dropped a third sum over all wave vectors), in different orbitals, and with opposite spin, as required by the dominant singlet pairing operator obtained from the numerical simulations. The potential is given by

$$V_{\mathbf{k},\mathbf{k}'} = -2V[\cos(k_x' - k_x) + \cos(k_y' - k_y)] = V(\mathbf{k}' - \mathbf{k}) = \sum_i \tilde{V}_i \eta_i(\mathbf{k}) \eta_i(\mathbf{k}'),$$

where $\eta_i(\mathbf{k})$ are the irreducible representations of the group D_{4h}. Since the ED numerical results indicate that the pairing operator is proportional to $(\cos k_x + \cos k_y)$, which corresponds to the irreducible representation A_{1g}, we will focus on that particular term in the expansion of the full potential $V_{\mathbf{k},\mathbf{k}'}$.[110] Thus, we will consider Eq. (A2) but using the long-range separable potential,

$$V_{\mathbf{k},\mathbf{k}'} = V^*(\cos k_x + \cos k_y)(\cos k_x' + \cos k_y'), \quad \text{(A3)}$$

instead of the full short-range potential.

We will treat the four-fermion term in H_{attr} within the usual mean-field approximation,[111] where some pairs of fermionic operators are replaced by numbers, such as $\langle b^{\dagger}_{\mathbf{k},\alpha}\rangle$, to be found self-consistently. Then

$$H_{\text{MF}} = H_{\text{TB}} + \sum_{\mathbf{k},\mathbf{k}',\alpha} (V_{\mathbf{k},\mathbf{k}'}\langle b^{\dagger}_{\mathbf{k},\alpha}\rangle d_{-\mathbf{k}',-\alpha,\downarrow} d_{\mathbf{k}',\alpha,\uparrow} + V_{\mathbf{k},\mathbf{k}'}\langle b_{\mathbf{k}',\alpha}\rangle d^{\dagger}_{\mathbf{k},\alpha,\uparrow} d^{\dagger}_{-k,-\alpha,\downarrow}) - \sum_{\mathbf{k},\mathbf{k}',\alpha} V_{\mathbf{k},\mathbf{k}'}\langle b^{\dagger}_{\mathbf{k},\alpha}\rangle\langle b_{\mathbf{k}',\alpha}\rangle. \quad \text{(A4)}$$

Defining

$$\Delta(\mathbf{k}) = -\sum_{\mathbf{k}',\alpha} V_{\mathbf{k},\mathbf{k}'}\langle b_{\mathbf{k}',\alpha}\rangle,$$

$$\Delta^{\dagger}(\mathbf{k}) = -\sum_{\mathbf{k}',\alpha} V_{\mathbf{k},\mathbf{k}'}\langle b^{\dagger}_{\mathbf{k}',\alpha}\rangle, \quad \text{(A5)}$$

and using the separability of the potential Eq. (A3), we obtain

$$H_{\text{MF}} = H_{\text{TB}} + \sum_{\mathbf{k},\alpha}[\Delta^{\dagger}(\mathbf{k}) d_{-k,-\alpha,\downarrow} d_{\mathbf{k},\alpha,\uparrow} \quad \text{(A6)}$$

$$+ \Delta(\mathbf{k}) d^{\dagger}_{\mathbf{k},\alpha,\uparrow} d^{\dagger}_{-\mathbf{k},-\alpha,\downarrow}] - \sum_{\mathbf{k},\mathbf{k}',\alpha} V_{\mathbf{k},\mathbf{k}'}\langle b^{\dagger}_{\mathbf{k},\alpha}\rangle \times\langle b_{\mathbf{k}',\alpha}\rangle, \quad \text{(A7)}$$

which leads to the same self-consistent equations as in Sec. V by setting

$$\Delta^{\dagger}(\mathbf{k}) = \Delta(\mathbf{k}) = V^*\Delta(\cos k_x + \cos k_y) \quad \text{(A8)}$$

and $V = V^*\Delta$, where Δ should be obtained by solving the gap equation that is obtained from minimizing the energy of the mean-field Hamiltonian with respect to $\Delta(\mathbf{k})$.

APPENDIX B: $s\pm$ PAIRING INVOLVING d_{xz} AND d_{yz} ELECTRONS

In Sec. IV B 2 we showed that our numerical simulations favored a spin-singlet interorbital pairing state with B_{2g} symmetry in the physical regime of parameters of the two-orbital model, while a pairing state with symmetry A_{1g} prevailed only in the unphysical strong coupling regime and at the singular point $U = U'$, $J = 0$. In this appendix we will discuss in more detail the pairing operators with A_{1g} symmetry in the context of the two-orbital model, and we will show that a $s\pm$ pairing operator[49,61,62,65] involving only d_{xz} and d_{yz} electrons belongs to this group.

The extensive literature on the $s\pm$ pairing state[49,61,62,65] indicates that this state does not have nodes on the Fermi surface and that

$$\Delta^1(\mathbf{k}) = -\Delta^2(\mathbf{k} + \mathbf{q}), \quad \text{(B1)}$$

where 1 (2) denotes the electron (hole) Fermi surface and $\mathbf{q} = (\pi, 0)$ or $(0, \pi)$.[65]

From the classification of possible pairing states for the d_{xz} and d_{yz} orbitals provided in Ref. 89 we realize that there exist the following four nodeless pairing operators: (i) pairing state 1 which produces on-site intraband pairs which are even under orbital exchange, spin singlets, and transforms according to the A_{1g} irreducible representation of D_{4h}. Following the steps of Sec. V A for this pairing state we obtain

$$H_{\text{MF}} = \begin{pmatrix} \xi_{xx} & \xi_{xy} & \Delta_0 & 0 \\ \xi_{xy} & \xi_{yy} & 0 & \Delta_0 \\ \Delta_0 & 0 & -\xi_{xx} & -\xi_{xy} \\ 0 & \Delta_0 & -\xi_{xy} & -\xi_{yy} \end{pmatrix}, \quad \text{(B2)}$$

where Δ_0 is a constant independent of momentum. In the base in which the tight-binding Hamiltonian is diagonal we obtain

$$H'_{\text{MF}} = \begin{pmatrix} \epsilon_1 & 0 & 0 & \Delta_0 \\ 0 & \epsilon_2 & \Delta_0 & 0 \\ 0 & \Delta_0 & -\epsilon_2 & 0 \\ \Delta_0 & 0 & 0 & -\epsilon_1 \end{pmatrix}. \quad \text{(B3)}$$

This leads to intraband pairing $\Delta_0 = V$ which is momentum independent and equal for the two bands. This does not correspond to the $s\pm$ pairing since it does not satisfy Eq. (B1).[65]

Now let us consider nearest-neighbor pairing. We find that the only nodeless pairing operators involving electrons in nearest-neighbor sites also have symmetry A_{1g} and result from a (ii) symmetric [or (iii) antisymmetric] combination of pairings 2 and 3. The symmetric (antisymmetric) combination corresponds to pairing of the d_{xz} electrons along the $x(y)$ direction while the d_{yz} pairs along the $y(x)$ direction. Following the steps of Sec. V A we obtain

$$H_{\text{MF}} = \begin{pmatrix} \xi_{xx} & \xi_{xy} & \Delta_1 & 0 \\ \xi_{xy} & \xi_{yy} & 0 & \Delta_2 \\ \Delta_1 & 0 & -\xi_{xx} & -\xi_{xy} \\ 0 & \Delta_2 & -\xi_{xy} & -\xi_{yy} \end{pmatrix}, \quad \text{(B4)}$$

where $\Delta_1 = V\cos k_x (V\cos k_y)$ and $\Delta_2 = V\cos k_y (V\cos k_x)$ for the symmetric (antisymmetric) combination. In the base in which the tight-binding Hamiltonian is diagonal we obtain

$$H'_{\mathrm{MF}} = \begin{pmatrix} \epsilon_1 & 0 & V_{12} & V_1 \\ 0 & \epsilon_2 & V_2 & V_{12} \\ V_{12} & V_2 & -\epsilon_2 & 0 \\ V_1 & V_{12} & 0 & -\epsilon_1 \end{pmatrix}, \tag{B5}$$

where V_1, V_2, and V_{12} are given by

$$V_1 = u^2\Delta_1 + v^2\Delta_2, \tag{B6}$$

$$V_2 = v^2\Delta_1 + u^2\Delta_2, \tag{B7}$$

$$V_{12} = uv(\Delta_1 - \Delta_2). \tag{B8}$$

Thus, this leads to intraband interactions V_1 and V_2 which, according to our numerical checks, satisfy $V_i(\mathbf{k}) = -V_i(\mathbf{k}+\mathbf{q})$ as expected for the $s\pm$ pairing,[65] but there is interband pairing given by V_{12} which is considered unphysical by many authors.[49,61,62,65]

(iv) Finally, we can also focus on pairs of electrons along the diagonals of the square lattice formed by the Fe ions. Following the notation in Ref. 89 the corresponding basis function is $\cos k_x \cos k_y$ that transforms according to A_{1g}. This basis provides a pairing operator with a full gap and which is a spin singlet. It is the analog of pairing 2 in Ref. 89 replacing the basis function $(\cos k_x + \cos k_y)$, which represents nearest-neighbor pairing and transforms according to A_{1g}, by $\cos k_x \cos k_y$ which corresponds to diagonal pairing and has the same symmetry. We will call this pairing $2'$. It transforms according to A_{1g} and it corresponds to intraorbital pairing. Following the previous steps we find that for pairing $2'$

$$H_{\mathrm{MF}} = \begin{pmatrix} \xi_{xx} & \xi_{xy} & \Delta_k & 0 \\ \xi_{xy} & \xi_{yy} & 0 & \Delta_k \\ \Delta_k & 0 & -\xi_{xx} & -\xi_{xy} \\ 0 & \Delta_k & -\xi_{xy} & -\xi_{yy} \end{pmatrix}, \tag{B9}$$

where $\Delta_k = V \cos k_x \cos k_y$, which is exactly the form of the $s\pm$ pairing interaction proposed in Ref. 65.

In the base in which the tight-binding Hamiltonian is diagonal we obtain

$$H'_{\mathrm{MF}} = \begin{pmatrix} \epsilon_1 & 0 & 0 & \Delta_k \\ 0 & \epsilon_2 & \Delta_k & 0 \\ 0 & \Delta_k & -\epsilon_2 & 0 \\ \Delta_k & 0 & 0 & -\epsilon_1 \end{pmatrix}. \tag{B10}$$

Note that this pairing operator corresponds to the $s\pm$ pairing since it satisfies $V_i(\mathbf{k}) = -V_i(\mathbf{k}+\mathbf{q})$ and there is no interband pairing. Thus, we have found that the $s\pm$ pairing operator is possible in the two-orbital model and transforms according to A_{1g}. However, the Lanczos numerical calculations presented in the text suggest that in the region of physical interest the undoped ground state has to be connected to the ground state with two extra electrons via a pairing operator that transforms according to B_{2g} and, for this reason, the $s\pm$ state is not favored. It only can prevail in the strong coupling regime of U and at the unphysical singular point $U=U'$, $J=0$ where the ground states in the doped and undoped regimes have the same symmetry and are connected by a pairing operator with A_{1g} symmetry.

For completeness, let us also consider a $s\pm$ pairing operator frequently used in the literature.[49,61,62,65] In this context it is assumed that $\Delta^1 = -\Delta^2 = \Delta_0$ which is independent of the momentum. Let us find whether this result is consistent with the symmetry of the two-orbital model. We start with H'_{MF} and working backward the form of H_{MF} is found. By this procedure we obtain

$$H'_{\mathrm{MF}} = \begin{pmatrix} \epsilon_1 & 0 & 0 & \Delta_0 \\ 0 & \epsilon_2 & -\Delta_0 & 0 \\ 0 & -\Delta_0 & -\epsilon_2 & 0 \\ \Delta_0 & 0 & 0 & -\epsilon_1 \end{pmatrix}, \tag{B11}$$

which in terms of the original two orbitals corresponds to

$$H_{\mathrm{MF}} = \begin{pmatrix} \xi_{xx} & \xi_{xy} & \Delta_{\mathrm{x}} & \Delta_{\mathrm{xy}} \\ \xi_{xy} & \xi_{yy} & \Delta_{\mathrm{xy}} & \Delta_{\mathrm{y}} \\ \Delta_{\mathrm{x}} & \Delta_{\mathrm{xy}} & -\xi_{xx} & -\xi_{xy} \\ \Delta_{\mathrm{xy}} & \Delta_{\mathrm{y}} & -\xi_{xy} & -\xi_{yy} \end{pmatrix}, \tag{B12}$$

where

$$\Delta_x = (u^2 - v^2)\Delta_0, \tag{B13}$$

$$\Delta_y = -(u^2 - v^2)\Delta_0, \tag{B14}$$

$$\Delta_{xy} = 2uv\Delta_0. \tag{B15}$$

We have found that uv transforms according to B_{1g} and $v^2 - u^2$ according to B_{2g}, then this case corresponds to a linear combination of on-site intraorbital (5) and interorbital (8) pairings that transform according to two different irreducible representations of D_{4h}, i.e., B_{1g} and B_{2g}. The coexistence of pairs with different symmetries can occur only if the ground state with N particles and/or the ground state with $N+2$ electrons are/is degenerate or nearly degenerate. Numerically, we have found that the ground states appear to be singlets and connected by an operator with symmetry B_{2g} in the region of physical relevance or A_{1g} in the strong coupling limit. Only in the unphysical singular point $J=0$ and $U=U'$ states transforming according to A_{1g}, B_{1g}, and B_{2g} are very close to each other in energy.

Summarizing, here it was shown that the $s\pm$ pairing operator that pairs electrons along the diagonals of the Fe square lattice using the d_{xz} and d_{yz} orbitals does transform according to the A_{1g} irreducible representation of the D_{4h} group that characterizes the symmetry of the Fe-As planes in the pnictides. Numerically we found that this is the pairing symmetry that prevails in the strong coupling region but that in the physical regime the pairing operator must transform according to B_{2g}. In addition, we have observed that the often-used momentum-independent approximation for the $s\pm$ operator does not respect the symmetry of the Fe-As planes.

[1] Y. Kamihara, T. Watanabe, M. Hirano, and H. Hosono, J. Am. Chem. Soc. **130**, 3296 (2008).
[2] G. F. Chen, Z. Li, G. Li, J. Zhou, D. Wu, J. Dong, W. Z. Hu, P. Zheng, Z. J. Chen, H. Q. Yuan, J. Singleton, J. L. Luo, and N. L. Wang, Phys. Rev. Lett. **101**, 057007 (2008).
[3] G. F. Chen, Z. Li, D. Wu, G. Li, W. Z. Hu, J. Dong, P. Zheng, J. L. Luo, and N. L. Wang, Phys. Rev. Lett. **100**, 247002 (2008).
[4] H.-H. Wen, G. Mu, L. Fang, H. Yang, and X. Zhu, EPL **82**, 17009 (2008).
[5] X. H. Chen, T. Wu, G. Wu, R. H. Liu, H. Chen, and D. F. Fang, Nature (London) **453**, 761 (2008).
[6] Z. A. Ren, J. Yang, W. Lu, W. Yi, G. C. Che, X. L. Dong, L. L. Sun, and Z. X. Zhao, Mater. Res. Innovations **12**, 105 (2008).
[7] R. Zhi-An, L. Wei, Y. Jie, Y. Wei, S. Xiao-Li, C. G.-C. Zheng-Cai, D. Xiao-Li, S. Li-Ling, Z. Fang, and Z. Zhong-Xian, Chin. Phys. Lett. **25**, 2215 (2008).
[8] Z.-A. Ren, G.-C. Che, X.-L. Dong, J. Yang, W. Lu, W. Yi, X.-L. Shen, Z.-C. Li, L.-L. Sun, F. Zhou, and Z.-X. Zhao, EPL **83**, 17002 (2008).
[9] L. Boeri, O. V. Dolgov, and A. A. Golubov, Phys. Rev. Lett. **101**, 026403 (2008).
[10] S. Higashitaniguchi, M. Seto, S. Kitao, Y. Kobayashi, M. Saito, R. Masuda, T. Mitsui, Y. Yoda, Y. Kamihara, M. Hirano, and H. Hosono, Phys. Rev. B **78**, 174507 (2008).
[11] A. D. Christianson, M. D. Lumsden, O. Delaire, M. B. Stone, D. L. Abernathy, M. A. McGuire, A. S. Sefat, R. Jin, B. C. Sales, D. Mandrus, E. D. Mun, P. C. Canfield, J. Y. Y. Lin, M. Lucas, M. Kresch, J. B. Keith, B. Fultz, E. A. Goremychkin, and R. J. McQueeney, Phys. Rev. Lett. **101**, 157004 (2008).
[12] A. S. Sefat, M. A. McGuire, B. C. Sales, R. Jin, J. Y. Howe, and D. Mandrus, Phys. Rev. B **77**, 174503 (2008).
[13] R. H. Liu, G. Wu, T. Wu, D. F. Fang, H. Chen, S. Y. Li, K. Liu, Y. L. Xie, X. F. Wang, R. L. Yang, L. Ding, C. He, D. L. Feng, and X. H. Chen, Phys. Rev. Lett. **101**, 087001 (2008).
[14] K. Haule, J. H. Shim, and G. Kotliar, Phys. Rev. Lett. **100**, 226402 (2008).
[15] K. Haule and G. Kotliar, New J. Phys. **11**, 025021 (2009).
[16] A. Dubroka, K. W. Kim, M. Rössle, V. K. Malik, A. J. Drew, R. H. Liu, G. Wu, X. H. Chen, and C. Bernhard, Phys. Rev. Lett. **101**, 097011 (2008).
[17] A. V. Boris, N. N. Kovaleva, S. S. A. Seo, J. S. Kim, P. Popovich, Y. Matiks, R. K. Kremer, and B. Keimer, Phys. Rev. Lett. **102**, 027001 (2009).
[18] C. Liu, T. Kondo, M. E. Tillman, R. Gordon, G. D. Samolyuk, Y. Lee, C. Martin, J. L. McChesney, S. Bud'ko, M. A. Tanatar, E. Rotenberg, P. C. Canfield, R. Prozorov, B. N. Harmon, and A. Kaminski, arXiv:0806.2147 (unpublished).
[19] Jun Zhao, Q. Huang, C. de la Cruz, S. Li, J. W. Lynn, Y. Chen, M. A. Green, G. F. Chen, G. Li, Z. Li, J. L. Luo, N. L. Wang, and P. Dai, Nature Mater. **7**, 953 (2008).
[20] Y. Kohama, Y. Kamihara, H. Kawaji, T. Atake, M. Hirano, and H. Hosono, J. Phys. Soc. Jpn. **77**, 094715 (2008).
[21] K. Nakamura, R. Arita, and M. Imada, J. Phys. Soc. Jpn. **77**, 093711 (2008).
[22] H. Liu, W. Zhang, L. Zhao, X. Jia, J. Meng, G. Liu, X. Dong, G. F. Chen, J. L. Luo, N. L. Wang, W. Lu, G. Wang, Y. Zhou, Y. Zhu, X. Wang, Z. Xu, C. Chen, and X. J. Zhou, Phys. Rev. B **78**, 184514 (2008).
[23] J. Jaroszynski, S. C. Riggs, F. Hunte, A. Gurevich, D. C. Larbalestier, G. S. Boebinger, F. F. Balakirev, A. Migliori, Z. A. Ren, W. Lu, J. Yang, X. L. Shen, X. L. Dong, Z. X. Zhao, R. Jin, A. S. Sefat, M. A. McGuire, B. C. Sales, D. K. Christen, and D. Mandrus, Phys. Rev. B **78**, 064511 (2008).
[24] M. M. Qazilbash, J. J. Hamlin, R. E. Baumbach, M. B. Maple, and D. N. Basov, arXiv:0808.3748 (unpublished).
[25] Y. Ishida, T. Shimojima, K. Ishizaka, T. Kiss, M. Okawa, T. Togashi, S. Watanabe, X. Y. Wang, C. T. Chen, Y. Kamihara, M. Hirano, H. Hosono, and S. Shin, Phys. Rev. B **79**, 060503(R) (2009).
[26] T. Sato, S. Souma, K. Nakayama, K. Terashima, K. Sugawara, T. Takahashi, Y. Kamihara, M. Hirano, and H. Hosono, J. Phys. Soc. Jpn. **77**, 063708 (2008).
[27] L. Hai-Yun, J. Xiao-Wen, Z. Wen-Tao, Z. Lin, M. Jian-Qiao, L. Guo-Dong, D. Xiao-Li, W. Gang, L. Rong-Hua, C. Xian-Hui, R. Zhi-An, Y. Wei, C. Guang-Can, C. Gen-Fu, W. Nan-Lin, W. Gui-Ling, Z. Yong, Z. Yong, W. Xiao-Yang, Z. Zhong-Xian, X. Zu-Yan, C. Chuang-Tian, and Z. Xing-Jiang, Chin. Phys. Lett. **25**, 3761 (2008).
[28] L. Zhao, H. Liu, W. Zhang, J. Meng, X. Jia, G. Liu, X. Dong, G. F. Chen, J. L. Luo, N. L. Wang, G. Wang, Y. Zhou, Y. Zhu, X. Wang, Z. Zhao, Z. Xu, C. Chen, and X. J. Zhou, Chin. Phys. Lett. **25**, 4402 (2008).
[29] A. J. Drew, F. L. Pratt, T. Lancaster, S. J. Blundell, P. J. Baker, R. H. Liu, G. Wu, X. H. Chen, I. Watanabe, V. K. Malik, A. Dubroka, K. W. Kim, M. Rössle, and C. Bernhard, Phys. Rev. Lett. **101**, 097010 (2008).
[30] I. Felner, I. Nowik, M. I. Tsindlekht, Z.-A. Ren, X.-L. Shen, G.-C. Che, and Z.-X. Zhao, arXiv:0805.2794 (unpublished).
[31] S. Takeshita, R. Kadono, M. Hiraishi, M. Miyazaki, A. Koda, Y. Kamihara, and H. Hosono, J. Phys. Soc. Jpn. **77**, 103703 (2008).
[32] H. Chen, Y. Ren, Y. Qiu, W. Bao, R. H. Liu, G. Wu, T. Wu, Y. L. Xie, X. F. Wang, Q. Huang, and X. H. Chen, EPL **85**, 17006 (2009).
[33] L. Shan, Y. Wang, X. Zhu, G. Mu, L. Fang, C. Ren, and H.-H. Wen, EPL **83**, 57004 (2008).
[34] M. Gang, Z. Xi-Yu, F. Lei, S. Lei, R. Cong, and W. Hai-Hu, Chin. Phys. Lett. **25**, 2221 (2008).
[35] C. Ren, Z.-S. Wang, H. Yang, X. Zhu, L. Fang, G. Mu, L. Shan, and H.-H. Wen, arXiv:0804.1726 (unpublished).
[36] K. Ahilan, F. L. Ning, T. Imai, A. S. Sefat, R. Jin, M. A. McGuire, B. C. Sales, and D. Mandrus, Phys. Rev. B **78**, 100501(R) (2008).
[37] Y. Nakai, K. Ishida, Y. Kamihara, M. Hirano, and H. Hosono, J. Phys. Soc. Jpn. **77**, 073701 (2008).
[38] H.-J. Grafe, D. Paar, G. Lang, N. J. Curro, G. Behr, J. Werner, J. Hamann-Borrero, C. Hess, N. Leps, R. Klingeler, and B. Büchner, Phys. Rev. Lett. **101**, 047003 (2008).
[39] Y.-L. Wang, L. Shan, L. Fang, P. Cheng, C. Ren, and H.-H. Wen, Supercond. Sci. Technol. **22**, 015018 (2009).
[40] K. Matano, Z. A. Ren, X. L. Dong, L. L. Sun, Z. X. Zhao, and Guo-qing Zheng, EPL **83**, 57001 (2008).
[41] H. Mukuda, N. Terasaki, H. Kinouchi, M. Yashima, Y. Kitaoka, S. Suzuki, S. Miyasaka, S. Tajima, K. Miyazawa, P. Shirage, H. Kito, H. Eisaki, and A. Iyo, J. Phys. Soc. Jpn. **77**, 093704 (2008).
[42] O. Millo, I. Asulin, O. Yuli, I. Felner, Z.-A. Ren, X.-L. Shen, G.-C. Che, and Z.-X. Zhao, Phys. Rev. B **78**, 092505 (2008).
[43] X. L. Wang, S. X. Dou, Z.-A. Ren, W. Yi, Z.-C. Li, Z.-X. Zhao, and S.-I. Lee, arXiv:0808.3398 (unpublished).

[44] K. Hashimoto, T. Shibauchi, T. Kato, K. Ikada, R. Okazaki, H. Shishido, M. Ishikado, H. Kito, A. Iyo, H. Eisaki, S. Shamoto, and Y. Matsuda, Phys. Rev. Lett. **102**, 017002 (2009).
[45] T. Kondo, A. F. Santander-Syro, O. Copie, C. Liu, M. E. Tillman, E. D. Mun, J. Schmalian, S. L. Bud'ko, M. A. Tanatar, P. C. Canfield, and A. Kaminski, Phys. Rev. Lett. **101**, 147003 (2008).
[46] H. Ding, P. Richard, K. Nakayama, K. Sugawara, T. Arakane, Y. Sekiba, A. Takayama, S. Souma, T. Sato, T. Takahashi, Z. Wang, X. Dai, Z. Fang, G. F. Chen, J. L. Luo, and N. L. Wang, EPL **83**, 47001 (2008).
[47] C. Martin, R. T. Gordon, M. A. Tanatar, M. D. Vannette, M. E. Tillman, E. D. Mun, P. C. Canfield, V. G. Kogan, G. D. Samolyuk, J. Schmalian, and R. Prozorov, arXiv:0807.0876 (unpublished).
[48] T. Y. Chen, Z. Tesanovic, R. H. Liu, X. H. Chen, and C. L. Chien, Nature (London) **453**, 1224 (2008).
[49] D. Parker, O. V. Dolgov, M. M. Korshunov, A. A. Golubov, and I. I. Mazin, Phys. Rev. B **78**, 134524 (2008).
[50] G. Mu, H. Luo, Z. Wang, L. Shan, C. Ren, and H.-H. Wen, arXiv:0808.2941 (unpublished).
[51] J. Dong, H. J. Zhang, G. Xu, Z. Li, G. Li, W. Z. Hu, D. Wu, G. F. Chen, X. Dai, J. L. Luo, Z. Fang, and N. L. Wang, EPL **83**, 27006 (2008).
[52] C. de la Cruz, Q. Huang, J. W. Lynn, W. Jiying Li, I. I. Ratcliff, J. L. Zarestky, H. A. Mook, G. F. Chen, J. L. Luo, N. L. Wang, and P. Dai, Nature (London) **453**, 899 (2008).
[53] Y. Chen, J. W. Lynn, J. Li, G. Li, G. F. Chen, J. L. Luo, N. L. Wang, P. Dai, C. dela Cruz, and H. A. Mook, Phys. Rev. B **78**, 064515 (2008).
[54] C. Krellner, N. Caroca-Canales, A. Jesche, H. Rosner, A. Ormeci, and C. Geibel, Phys. Rev. B **78**, 100504(R) (2008).
[55] A. I. Goldman, D. N. Argyriou, B. Ouladdiaf, T. Chatterji, A. Kreyssig, S. Nandi, N. Ni, S. L. Bud'ko, P. C. Canfield, and R. J. McQueeney, Phys. Rev. B **78**, 100506(R) (2008).
[56] S. Lebegue, Phys. Rev. B **75**, 035110 (2007).
[57] D. J. Singh and M.-H. Du, Phys. Rev. Lett. **100**, 237003 (2008).
[58] G. Xu, W. Ming, Y. Yao, X. Dai, S.-C. Zhang, and Z. Fang, EPL **82**, 67002 (2008).
[59] C. Cao, P. J. Hirschfeld, and H. P. Cheng, Phys. Rev. B **77**, 220506(R) (2008).
[60] H.-J. Zhang, G. Xu, X. Dai, and Z. Fang, Chin. Phys. Lett. **26**, 017401 (2009).
[61] K. Kuroki, S. Onari, R. Arita, H. Usui, Y. Tanaka, H. Kontani, and H. Aoki, Phys. Rev. Lett. **101**, 087004 (2008).
[62] I. I. Mazin, D. J. Singh, M. D. Johannes, and M. H. Du, Phys. Rev. Lett. **101**, 057003 (2008).
[63] X. Dai, Z. Fang, Y. Zhou, and F.-C. Zhang, Phys. Rev. Lett. **101**, 057008 (2008).
[64] Q. Han, Y. Chen, and Z. D. Wang, EPL **82**, 37007 (2008).
[65] M. M. Korshunov and I. Eremin, Phys. Rev. B **78**, 140509(R) (2008).
[66] G. Baskaran, arXiv:0804.1341 (unpublished).
[67] P. A. Lee and X.-G. Wen, arXiv:0804.1739 (unpublished).
[68] T. Yildirim, Phys. Rev. Lett. **101**, 057010 (2008).
[69] Q. Si and E. Abrahams, Phys. Rev. Lett. **101**, 076401 (2008).
[70] Z.-J. Yao, J.-X. Li, and Z.-D. Wang, New J. Phys. **101**, 076401 (2008).
[71] C. Xu, M. Müller, and S. Sachdev, Phys. Rev. B **78**, 020501(R) (2008).
[72] E. Manousakis, J. Ren, S. Meng, and E. Kaxiras, Phys. Rev. B **78**, 205112 (2008).
[73] S. Raghu, X. L. Qi, C. X. Liu, D. J. Scalapino, and S. C. Zhang, Phys. Rev. B **77**, 220503(R) (2008).
[74] T. Li, J. Phys.: Condens. Matter **20**, 425203 (2008).
[75] X.-L. Qi, S. Raghu, C.-X. Liu, D. J. Scalapino, and S.-C. Zhang, arXiv:0804.4332 (unpublished).
[76] M. Daghofer, A. Moreo, J. A. Riera, E. Arrigoni, D. J. Scalapino, and E. Dagotto, Phys. Rev. Lett. **101**, 237004 (2008).
[77] K. Seo, B. A. Bernevig, and J. Hu, Phys. Rev. Lett. **101**, 206404 (2008).
[78] Y. Ran, F. Wang, H. Zhai, A. Vishwanath, and D.-H. Lee, Phys. Rev. B **79**, 014505 (2009).
[79] Y. Zhou, W.-Q. Chen, and F.-C. Zhang, Phys. Rev. B **78**, 064514 (2008).
[80] J. Lorenzana, G. Seibold, C. Ortix, and M. Grilli, Phys. Rev. Lett. **101**, 186402 (2008).
[81] R. Sknepnek, G. Samolyuk, Y.-bin Lee, and J. Schmalian, Phys. Rev. B **79**, 054511 (2009).
[82] M. M. Parish, J. Hu, and B. A. Bernevig, Phys. Rev. B **78**, 144514 (2008).
[83] H.-Y. Choi and Y. Bang, arXiv:0807.4604 (unpublished).
[84] S. Yang, W.-L. You, S.-J. Gu, and H.-Q. Lin, arXiv:0807.0587 (unpublished).
[85] M. J. Calderon, B. Valenzuela, and E. Bascones, New J. Phys. **11**, 013051 (2009).
[86] Z.-H. Wang, H. Tang, Z. Fang, and X. Dai, arXiv:0805.0736 (unpublished).
[87] J. Shi, arXiv:0806.0259 (unpublished).
[88] W.-L. You, S.-J. Gu, G.-S. Tian, and H.-Q. Lin, arXiv:0807.1493 (unpublished).
[89] Y. Wan and Q.-H. Wang, arXiv:0805.0923 (unpublished).
[90] A. Kawabata, S. C. Lee, T. Moyoshi, Y. Kobayashi, and M. Sato, arXiv:0807.3480 (unpublished).
[91] V. Vildosola, L. Pourovskii, R. Arita, S. Biermann, and A. Georges, Phys. Rev. B **78**, 064518 (2008).
[92] H. Suhl, B. T. Matthias, and L. R. Walker, Phys. Rev. Lett. **3**, 552 (1959).
[93] J. C. Slater and G. F. Koster, Phys. Rev. **94**, 1498 (1954).
[94] For more details, see P. Fulde, *Electron Correlations in Molecules and Solids*, Springer Series in Solid-State Sciences Vol. 100 (Springer, Berlin, 1991).
[95] W. A. Harrison, *Electronic Structure and the Properties of Solids* (Dover, New York, 1989).
[96] E. Dagotto, T. Hotta, and A. Moreo, Phys. Rep. **344**, 1 (2001).
[97] E. Dagotto, Rev. Mod. Phys. **66**, 763 (1994).
[98] For small $|pd\pi|<0.15$, we find other states. They have p symmetry and their momentum is (π,π) instead of (0, 0). Since these parameters locate us close to the phase transition of the half-filled system at $pd\pi\approx 0$, where the Fermi surface topology changes [see Fig. 9(d)] and the crucial $(0,\pi)$ spin order breaks down [see Fig. 11(a)], we tentatively attribute these exotic results with finite-momentum pairing to finite size effects.
[99] N. Kumar and K. P. Sinha, Phys. Rev. **174**, 482 (1968).
[100] Jamil Tahir-Kheli, Phys. Rev. B **58**, 12307 (1998).
[101] O. V. Dolgov, E. P. Fetisov, D. I. Khomskii, and K. Svozil, Z. Phys. B: Condens. Matter **67**, 63 (1987).
[102] R. Yu, K. Trinh, A. Moreo, M. Daghofer, J. Riera, S. Haas, and E. Dagotto, Phys. Rev. B **79**, 104510 (2009).
[103] Another way to understand the "nontrivial" nodes in the MF solution is the following: if $\xi_{xy}=0$, which happens if $\sin(k_i)=0$

(for $i=x$ or y) as already discussed, then the original Hamiltonian (28) has a simple form. The nodes will occur at values of (k_x,k_y) where the determinant of Eq. (28) with $\xi_{xy}=0$ vanishes. The resulting equation is given by $\Delta_k^2+\xi_{xx}\xi_{yy}=0$. Note now that ξ_{ii} and Δ_k are only functions of $\cos k_x$ or $\cos k_y$ since one of these cosines is fixed to 1 or -1 due to $\xi_{xy}=0$. The product $\xi_{xx}\xi_{yy}$ has to be negative indicating that, if the resulting quadratic equation has real solutions, the nodes will appear at points that lie in between the two noninteracting Fermi surfaces, as derived before.

[104] L. Wray, D. Qian, D. Hsieh, Y. Xia, L. Li, J. G. Checkelsky, A. Pasupathy, K. K. Gomes, A. V. Fedorov, G. F. Chen, J. L. Luo, A. Yazdani, N. P. Ong, N. L. Wang, and M. Z. Hasan, arXiv:0808.2185 (unpublished). In Ref. 18 it was also concluded that the regime of strong coupling was realized in the Fe pnictides.

[105] A similar conclusion regarding the importance of further analyzing the electron pockets holds for the ARPES study reported in Ref. 28.

[106] V. B. Zabolotnyy, D. S. Inosov, D. V. Evtushinsky, A. Koitzsch, A. A. Kordyuk, J. T. Park, D. Haug, V. Hinkov, A. V. Boris, D. L. Sun, G. L. Sun, C. T. Lin, B. Keimer, M. Knupfer, B. Buechner, A. Varykhalov, R. Follath, and S. V. Borisenko, Nature (London) **457**, 569 (2009).

[107] We have observed that pairing 8 (B_{2g} on site) that, as mentioned in the text, appears to coexist with pairing 9 (B_{2g} nearest neighbors) produces a nodeless gap for some values of V. However, only combinations of pairings 8 and 9 in which V is stronger for 8 provide a nodeless gap while the numerical results appear to indicate that V should be smaller for 8.

[108] F. Krüger, S. Kumar, J. Zaanen, and J. van den Brink, Phys. Rev. B **79**, 054504 (2009).

[109] See, for instance, E. Dagotto, J. Riera, Y. C. Chen, A. Moreo, A. Nazarenko, F. Alcaraz, and F. Ortolani, Phys. Rev. B **49**, 3548 (1994); A. Nazarenko, Adriana Moreo, Elbio Dagotto, and Jose Riera, *ibid.* **54**, R768 (1996), and references therein.

[110] R. Fehrenbacher and M. R. Norman, Phys. Rev. Lett. **74**, 3884 (1995).

[111] J. Schrieffer, *Theory of Superconductivity*, 4th ed. (Addison-Wesley, New York, 1988).